HHS Public Access

Author manuscript

Circulation. Author manuscript; available in PMC 2020 April 16.

Published in final edited form as:

Circulation. 2019 April 16; 139(16): 1913–1936. doi:10.1161/CIRCULATIONAHA.118.033552.

Hyperglycemia-driven Inhibition of AMP-Activated Protein Kinase α2 Induces Diabetic Cardiomyopathy by Promoting Mitochondria-associated Endoplasmic Reticulum Membranes *in vivo*

Shengnan Wu, PhD[1], **Qiulun Lu, PhD**[1], **Ye Ding, PhD**[1], **Yin Wu, MS**[1], **Yu Qiu, MS**[1], **Pei Wang, PhD**[2], **Xiaoxiang Mao, MD**[3], **Kai Huang, MD, PhD**[3], **Zhonglin Xie, MD PhD**[1,#], and **Ming-Hui Zou, MD PhD**[1,#]

[1]Center for Molecular and Translational Medicine, Georgia State University, Atlanta, GA, 30303

[2]Mitochondria and Metabolism Center, 850 Republican Street, University of Washington, Seattle, WA

[3]Wuhan Union Hospital, Huazhong University of Science and Technology, Wuhan, Hubei, China

Abstract

Background—FUN14 domain containing 1 (Fundc1), an outer mitochondrial membrane protein, is important for mitophagy and mitochondria-associated endoplasmic reticulum (ER) membranes (MAMs). The roles of Fundc1 and MAMs in diabetic hearts remain unknown. The aims of this study therefore, were to determine if the diabetes-induced Fundc1 expression could increase MAM formation, and whether disruption of MAM formation improves diabetic cardiac function.

Methods—Levels of FUNDC1 were examined in the hearts from diabetic patients and non-diabetic donors. Levels of Fundc1-induced MAMs, and mitochondrial and heart function were examined in mouse neonatal cardiomyocytes exposed to high glucose (HG, 30 mmol/L D-glucose for 48 h), as well as in streptozotocin (STZ)-treated cardiac-specific *Fundc1* knockout (KO) mice and cardiac-specific *Fundc1* KO diabetic Akita mice.

Results—FUNDC1 levels were significantly elevated in cardiac tissues from diabetic patients compared to those in non-diabetic donors. In cultured mouse neonatal cardiomyocytes, HG conditions increased levels of Fundc1, the inositol 1,4,5-trisphosphate type 2 receptor (Ip_3r2), and MAMs. Genetic downregulation of either Fundc1 or Ip_3r2 inhibited MAM formation, reduced ER-mitochondrial Ca^{2+} flux, and improved mitochondrial function in HG-treated cardiomyocytes. Consistently, adenoviral overexpression of *Fundc1* promoted MAM formation, mitochondrial Ca^{2+} increase, and mitochondrial dysfunction in cardiomyocytes exposed to normal glucose (5.5 mmol/L D-glucose). Compared with non-diabetic controls, levels of Fundc1, Ip_3r2, and MAMs were significantly increased in hearts from STZ-treated mice and Akita mice. Further, compared

[#]Address correspondence to: Ming-Hui Zou, MD PhD or Dr. Zhonglin Xie, MD PhD, Center for Molecular and Translational Medicine, Georgia State University, 157 Decatur Street North East, Phone: 404-413-6637, Fax: 404-413-3580, mzou@gsu.edu, zxie@gsu.edu.

Disclosures

None.

with control hearts, diabetes markedly increased co-immunoprecipitation of Fundc1 and Ip_3r2. The binding of Fundc1 to Ip_3r2 inhibits Ip_3r2 ubiquitination and proteasome-mediated degradation. Cardiomyocyte-specific *Fundc1* deletion ablated diabetes-induced MAM formation, prevented mitochondrial Ca^{2+} increase, mitochondrial fragmentation, and apoptosis with improved mitochondrial functional capacity and cardiac function. In mouse neonatal cardiomyocytes, HG suppressed AMP-activated protein kinase (Ampk) activity. Furthermore, in cardiomyocytes of *Prkaa2* KO mice, expression of Fundc1, MAM formation, and mitochondrial Ca^{2+} levels were significantly increased. Finally, adenoviral overexpression of a constitutively active mutant Ampk ablated HG-induced MAM formation and mitochondrial dysfunction.

Conclusions—We conclude that diabetes suppresses Ampk, initiating Fundc1-mediated MAM formation, mitochondrial dysfunction, and cardiomyopathy, suggesting that Ampk-induced Fundc1 suppression is a valid target to treat diabetic cardiomyopathy.

Keywords

Cardiomyopathy; MAMs; Fundc1; Mitochondrial dysfunction; Ampk

Introduction

Diabetic cardiomyopathy is a major cause of heart failure and death in patients with diabetes. Although hyperglycemia or high glucose (HG), a pathologic factor in type 1 diabetes, promotes the development of diabetic cardiomyopathy, the exact mechanisms by which it affects pathological processes are poorly characterized. Mitochondria are essential for cellular energy production, but if damaged, they become a major source of reactive oxygen species (ROS) and pro-apoptotic factors. In particular, increasing evidence suggests that mitochondrial dysfunction is a central event in diabetic cardiomyopathy[1, 2]. Although mitochondria are implicated in diabetic cardiomyopathy, the molecular mechanisms by which diabetes impairs mitochondrial function remain elusive[3-6].

The mitochondria and endoplasmic reticulum (ER) are key players that regulate many cellular functions[7], and their structural and functional interactions are essential for cellular homeostasis[7]. The contact points through which the ER communicates with mitochondria are known as mitochondria-associated ER membranes (MAMs).[7] MAMs are enriched in phospholipid- and glycosphingolipid-synthesis enzymes and chaperone proteins, and the tethering of MAMs is executed by several molecular bridges.[8] For example, inositol 1,4,5-trisphosphate receptors (Ip_3rs) interact with the voltage-dependent anion-selective channel 1 (Vdac1) to form an ER-mitochondria calcium (Ca^{2+}) tunnel.[9] The mitochondrial outer membrane protein mitofusin 2 (Mfn2) tethers the ER to mitochondria by forming homotypic or heterotypic complexes with mitochondrial Mfn1/2.[10] Recently, we reported a new protein bridge, formed through the interaction of a the outer mitochondrial membrane human protein FUN14 domain containing 1 (Fundc1) with the ER protein inositol 1,4,5-trisphosphate type 2 receptor (Ip_3r2)[11]. Importantly, MAMs play a pivotal role in Ca^{2+} signaling, lipid transport, energy metabolism, and cell survival[12], and have been implicated in disease, including Alzheimer's disease[13], cancer[14], lysosomal storage disease[15], diabetes[16, 17], obesity-induced mitochondrial dysfunction, and metabolic disorders[18].

However, the role of MAMs in the initiation and progression of diabetic cardiomyopathy remain unknown.

Due to its role in excitation-contraction coupling in muscle tissue, Ca^{2+} signaling is crucial for appropriate heart function, and Ca^{2+} increase has been implicated in heart failure associated with several pathological conditions. During ischemia/reperfusion, cytosolic Ca^{2+} accumulation causes mitochondrial Ca^{2+} increase, which activates the matrix chaperone cyclophilin D (CypD) and triggers the opening of the permeability transition pore, leading to cell death.[19] Interestingly, decreasing ER-mitochondria tethering can prevent this increase and subsequent cell death.[20] Defects in intracellular Ca^{2+} homeostasis have been implicated in diabetic cardiac dysfunction[21, 22]; however, the exact mechanisms for diabetes-induced Ca^{2+} homeostasis disruption remain unclear.

Fundc1 is a highly conserved protein exclusively localized to the mitochondria. It possesses a hydrophobic transmembrane domain consisting of three α-helices, with a cytosol-exposed amino terminus and a carboxyl terminus that spans the intermembrane space. Fundc1 contains a microtubule-associated protein 1A/1B-light chain 3 (Lc3)-binding motif that interacts with Lc3 and recruits mitochondria to autophagosomes.[23, 24] Fundc1 can also promote mitochondrial fission by directly interacting with dynamin-related protein 1 (Drp1) at ER-mitochondria contact sites.[25] Our previous work demonstrated that Fundc1 is essential for maintaining the structure of MAMs and ensuring appropriate Ca^{2+} transfer from the ER to mitochondria in normal hearts.[11] Moreover, cardiac-specific deletion of *Fundc1* induces cardiac dysfunction by inhibiting MAM formation.[11] However, whether or not Fundc1-related MAMs contribute to diabetic cardiomyopathy remains to be determined. Here, we report that HG-driven inactivation of AMP-activated protein kinase (Ampk) increases Fundc1 stability, resulting in aberrant MAM formation, mitochondrial Ca^{2+} increase, mitochondrial dysfunction, and cardiac dysfunction. Additionally, Ampk activation reverses diabetic cardiomyopathy by suppressing HG-induced MAM formation, mitochondrial Ca^{2+} increase, and mitochondrial dysfunction.

Methods

The data, analytical methods, and study materials will be made available to other researchers for purposes of reproducing the results or replicating the procedure and are available by contacting the corresponding authors.

Human Samples

FUNDC1 expression was examined in the left ventricle cardiac tissues of hearts from patients with clinically diagnosed diabetic cardiomyopathy (recipients) and healthy human donor hearts. All human studies were approved by the human ethics committee of Wuhan Union Hospital of Huazhong University of Science and Technology (2017-S10005), and the subjects provided informed consent. Patient characteristics are summarized in Supplemental Table 1.

Animal Study Approval

The animal protocol in this study was approved by the Institutional Animal Care and Use Committee (IACUC) at Georgia State University.

Generation of Cardiomyocyte-Specific *Fundc1* Knockout (KO) Akita Mice

Mice expressing a floxed *Fundc1* gene (on the X chromosome) were developed by the Mouse Biology Program at the University of California, Davis. C57BL/6J wild-type (WT), $Cre^{\alpha MyHC+/-}$, and diabetic heterozygous Akita ($Ins2^{wt/C96Y}$)[26] mice were purchased from the Jackson Laboratory (Bar Harbor, ME). The $Cre^{\alpha MyHC+/-}$ allele allows Cre recombinase expression specifically in cardiomyocytes under control of the cardiac-specific alpha myosin heavy chain (αMyHC) promoter. Cardiomyocyte-specific *Fundc1* KO ($Fundc1^{f/Y}/Cre^{\alpha MyHC+/-}$) mice were generated by crossing $Fundc1^{wt/f}/Cre^{\alpha MyHC+/-}$ with $Fundc1^{wt/Y}/Cre^{\alpha MyHC+/-}$ mice. Littermate $Fundc1^{wt/Y}/Cre^{\alpha MyHC+/-}$ mice were used as controls. Male heterozygous Akita ($Ins2^{wt/C96Y}$) mice were crossed with female $Fundc1^{f/f}/Cre^{\alpha MyHC+/-}$ mice to obtain *Fundc1* KO Akita ($Fundc1^{f/Y}/Cre^{\alpha MyHC+/-}/Ins2^{wt/C96Y}$) double mutants. All mice were maintained in a C57BL/6J background, housed in temperature-controlled cages with a 12 h light-dark cycle, and given free access to water and food. The mice were used for experiments at 6 months of age. Akita mice were purchased from Jackson Laboratory (Bar Harbor, ME), and 6-month-old male mice were used for the experiments.

Screening $Nnt^{+/+}$ Mice

Nicotinamide nucleotide transhydrogenase (Nnt) mutation affects the redox state of mitochondria, and thus may affect mitochondrial function.[27, 28] PCR was used to detect *Nnt* mutation in all mice used in 6 lines (littermates: WT, *Fundc1* KO, Akita, *Fundc1* KO-Akita, and littermates: WT and *Prkaa2* KO) used in this study. All six lines carry *Nnt* mutation ($Nnt^{+/-}$) in a random way. To exclude potential effects of *Nnt* mutation on our results, all mice which carried *Nnt* mutation were removed from this study.

Induction of Diabetes

Type 1 diabetes was induced by streptozotocin (STZ) injection following the Low-Dose Streptozotocin Induction Protocol (Mouse) published by Animal Models of Diabetic Complications Consortium. Briefly, type 1 diabetes was induced in 8-week-old $Fundc1^{wt/Y}/Cre^{\alpha MyHC+/-}$ (WT) and $Fundc1^{f/Y}/Cre^{\alpha MyHC+/-}$ (KO) mice via daily STZ (Sigma-Aldrich, St. Louis, MO) intraperitoneal injections (50 mg/kg in citrate buffer, pH 4.5) for 5 consecutive days. Control mice received citrate buffer injections (vehicle). Blood glucose was measured 2 weeks post-injection, and only animals with blood glucose levels greater than 350 mg/dL were considered diabetic. Mice were used for experiments four months post-induction.

Echocardiography

Mouse cardiac geometry and function were examined using a Vevo 3100 High-Resolution Micro-Ultrasound System (FUJIFILM Visual Sonics Inc., Toronto, ON, Canada). Mice were anesthetized with 1.5% isoflurane and placed on a heating table in a supine position. Two-

dimensional images of the cardiac chamber were obtained from short-axis views of the left ventricle at the papillary muscle level. Left ventricular (LV) internal diameter (LVID), posterior wall thickness (LVPW), fractional shortening (FS), and ejection fractions (EF) were calculated from the left ventricular dimensions at the end of systole and diastole. Diastolic dysfunction was also assessed using the ratio of early (E-wave) and late (A-wave) LV diastolic filling velocities (E/A ratio), determined by transmitral valve Doppler. To avoid bias, all echocardiography procedures, including data acquisition and analysis, were performed by a researcher who was blind to the experimental treatments.

Cell Culture

Mouse neonatal cardiomyocytes were isolated from 1- to 3-day-old mice using a Primary Cardiomyocyte Isolation Kit (#88281; Thermo Fisher Scientific Inc., Waltham, MA). Briefly, freshly isolated hearts were minced and incubated with isolation enzymes for 35 min, and then washed twice with Hanks Balanced Salt Solution. The tissues were disrupted in Dulbecco's Modified Eagle Medium (DMEM) specific for primary cell isolation (#88287, Thermo Fisher Scientific Inc., Waltham, MA) supplemented with 10% fetal bovine serum (FBS), penicillin (100 U/mL), and streptomycin (100 μg/mL), and cardiomyocyte growth supplement (provided by manufacturer diluted at a ratio 1: 1000), by pipetting up and down 25 to 30 times with a 1000 μL pipette tip to generate a single cell suspension. Total cell yield was determined using a TC20™ Automated Cell Counter (Bio-Rad Laboratories, Inc., Hercules, CA), and cell viability was determined using a Trypan Blue exclusion assay. The isolated cardiomyocytes were maintained in DMEM supplemented with 10% FBS, penicillin (100 U/mL), and streptomycin (100 μg/mL).

Adult cardiac myocytes were isolated from female C57BL/6J mice following the protocol reported previously[29]. Briefly, the mouse was anesthetized by intraperitoneal injection of pentobarbital. The heart was quickly removed, cannulated via ascending aorta, and mounted on a modified Langendorff perfusion system. The heart was perfused with oxygenated Krebs-Henseleit Buffer (KHB) solution supplemented with collagenase II (Worthington) and hyaluronidase (Sigma) at 37°C. Rod-shaped adult cardiac myocytes were collected and plated on glass coverslips coated with laminin at a density of 2×10^4 cells per coverslip and cultured in serum-free M199 medium (Sigma) supplemented with 10 mM glutathione, 26.2 mM sodium bicarbonate, 0.02% bovine serum albumin and 50 U/ml penicillin-streptomycin for up to 3 days.

Rat H9c2 cardiomyoblasts (ATCC®CRL-1446™) were purchased from American Type Culture Collection (Rockville, MD), maintained in DMEM (#11885, Thermo Fisher Scientific Inc., Waltham, MA), supplemented with 10% FBS, and were incubated in a humidified atmosphere with 5% CO_2 and 95% air at 37°C. All culture media were supplemented with penicillin (100 U/mL) and streptomycin (100 μg/mL).

Plasmid Transfection, Gene Silencing, and Adenovirus Infection

The DsRed2-ER (#632409) plasmid was purchased from Clontech Laboratories, Inc. (Mountain View, CA). GFP-Fundc1Δ7-48 mutation plasmid was generated using Quikchange II Site-directed Mutagenesis Kit (Agilent Cat: 200523). The procedure was

followed with the company protocol. The GFP-Fundc1 plasmid (Origene Cat: RG208211) was used to delete region 7-48. The resulting plasmid was sequenced and confirmed with T7 primer. Cardiomyocytes were transfected with plasmids using Lipofectamine 2000 (#11668-019, Life Technologies, Carlsbad, CA), according to the manufacturer's protocol.

Fundc1 siRNA (#sc-145273) was purchased from Santa Cruz Biotechnology, Inc. (Dallas, Texas). *Itpr2* siRNA (#n435663) was purchased from Life Technologies. For gene silencing of *Fundc1* or *Itpr2*, cardiomyocytes were transfected with 10 μmol/L siRNA using Lipofectamine®RNAiMAX (#13778150, Life Technologies, Carlsbad, CA) according to the instructions provided by the supplier.

The mouse neonatal cardiomyocytes or H9c2 myoblasts were infected with adenovirus encoding Fundc1 (#197503A and #281786A, Applied Biological Materials Inc., Canada) in normal culture medium for 48 h. An adenoviral vector encoding beta-galactosidase (β-Gal) (#000197A, Applied Biological Materials Inc., Canada) was used as a control. Adenovirus encoding constitutively active Ampk mutants (ad-Ampk-CA) was generated as described earlier[30].

Immunoprecipitation and Western Blot

Cultured cardiomyocytes and cardiac tissues (whole heart) were homogenized in radioimmunoprecipitation assay (RIPA) lysis buffer (#sc-24948, Santa Cruz Biotechnology, Inc., Dallas, Texas). RIPA buffer contained 200 mmol/L phenylmethylsulfonyl fluoride (PMSF), protease inhibitor cocktail, and detergents (including ionic detergents: sodium dodecyl sulfate [SDS] and 100 mmol/L sodium deoxycholate, and non-ionic detergent Nonidet P-40). The protein contents were measured using a bicinchoninic acid assay (BCA, #23225, Pierce Biotechnology, Rockford, IL). Total cell lysates were immunoprecipitated with specific antibodies, and the immunoprecipitates were subjected to western blot. For western blot analysis, 40~80 μg of protein was resolved by sodium dodecyl sulfate polyacrylamide gel electrophoresis (SDS-PAGE), transferred to nitrocellulose (NC) membranes (Bio-Rad Laboratories, Inc. Hercules, CA), and probed with specific antibodies. The signals were visualized using Amersham Imager 680 (GE Healthcare, Piscataway, NJ). The intensity (area × density) of individual bands was measured by densitometry (ImageQuant TL 8.2 image analysis software, GE Healthcare Life Sciences), and the background was subtracted from the calculated area. The following primary antibodies were used: anti-FUNDC1 (#NBP1-81063, Novus Biologicals, LLC, Littleton CO), anti-FUNDC1 (#ABC506, EMD Millipore Corporation, Temecula, CA), anti-IP_3R2 (#ab55981, Abcam, Cambridge, MA), anti-IP_3R2 (#sc-398434, Santa Cruz Biotechnology, Inc., Dallas, Texas), anti-PACS2 (#19508-1-AP, Proteintech, Chicago, IL), anti-Sig1r (#42-3300, Thermo Fisher Scientific Inc., Waltham, MA), anti-MFN2 (#sc-50331, Santa Cruz Biotechnology, Inc., Dallas, Texas), anti-PDI (#2446, Cell Signaling Technology, Inc., Danvers, MA), anti-GRP75 (#2816, Cell Signaling Technology, Inc., Danvers, MA), anti-VDAC1 (#4661, Cell Signaling Technology, Inc., Danvers, MA), anti-CALRETICULIN (#ab39818, Abcam, Cambridge, MA), anti-β-Tubulin (#AC02, ABclonal, Inc. Woburn, MA), anti-GAPDH (#sc-137179, Santa Cruz Biotechnology, Inc., Dallas, Texas), anti-UB (#sc-8017, Santa Cruz Biotechnology, Inc., Dallas, Texas), anti-RNF170 (#ab80435, Abcam, Cambridge, MA),

anti-β-Actin (#sc-47778, Santa Cruz Biotechnology, Inc., Dallas, Texas), anti-Phospho-AMPKα (Thr172) (#2535, Cell Signaling Technology, Inc., Danvers, MA), anti-AMPKα2 (#sc-19131, Santa Cruz Biotechnology, Inc., Dallas, Texas), anti-Phospho-Acc (Ser79) (#3661, Cell Signaling Technology, Inc., Danvers, MA), anti-β-MHC (#22280-1-AP, Proteintech, Chicago, IL), anti-TNF-α (#sc-1351, Santa Cruz Biotechnology, Inc., Dallas, Texas), and anti-IL-6 (#sc-12912, Cell Signaling Technology, Inc., Danvers, MA).

Subcellular Fractionation

Subcellular fractionation of the heart was performed using published protocols[31].

Mitochondria Isolation from Heart

Mitochondria used for FCM analysis were isolated using a Mitochondria Isolation Kit (#89801, Thermo Fisher Scientific Inc., Waltham, MA). Each heart was washed twice with 2 ml phosphate-buffered saline (PBS), and the PBS was then discarded. The heart tissue was cut into small pieces (less than 1×1×1 mm^3), which were incubated on ice in a trypsin/PBS solution (0.3 mg/ml) for 3 min followed by brief centrifugation at 250 × *g* for 1 min at 4°C to pellet the tissue and remove the trypsin solution. We added 800 μL 4 mg/ml BSA/Reagent A solution (with protease inhibitors) to the tube, and Dounce homogenization was performed on ice. We then added 800 μL Reagent C (with protease inhibitors) and inverted the tube several times to mix. The tubes were centrifuged at 700 × *g* for 10 min at 4°C, and the pellet was discarded. The supernatant was then centrifuged at 3,000 × *g* for 15 min at 4°C, and 500 μl wash buffer (Reagent C with an equal volume of ultrapure water) was added to the mitochondrial pellet. The ultrapure water was prepared by Milli-Q® Reference Water Purification System (MilliporeSigma Life Science, Burlington, MA) with a resistivity of 18.2 MΩ•cm at 25°C, and total organic carbon ≤ 5 ppb. The mitochondrial pellet was centrifuged at 12,000 × *g* for 5 min and stored on ice before downstream processing. The quality (purity and activity) of the isolated mitochondria was determined by FCM based on double staining with MitoTracker Green and tetramethylrhodamine, methyl ester (TMRM).

Immunofluorescence

Cells were washed twice with PBS, fixed with 3.7% paraformaldehyde (v/v) in PBS for 15 min, and permeabilized with 0.2% Triton X-100 (v/v) for 15 min. Cells were blocked with 5% normal goat serum (BioGenex, Fremont, CA) for 30 min, incubated with primary antibodies (1: 200) at 37°C for 30 min, followed by incubation with Alexa Fluor® 488- or 647-conjugated secondary antibodies (1:50) (Life Technologies, Carlsbad, CA) at 37°C for 45 min. The cover slips were mounted on microscope slides using an anti-fade medium and sealed before imaging. Images were obtained using a confocal microscope (LSM800, Carl Zeiss Microscopy Ltd., Cambridge, MA).

ER and Mitochondria Contact Analysis

Cells were transfected with a DsRed2-ER plasmid (Ex/Em 558/583 nm; #632409, Clontech Laboratories, Inc., Mountain View, CA) for 48 h, labeled with MitoTracker® Green FM (250 nm, Ex/Em 490/516 nm; #7514, Thermo Fisher Scientific Inc. Waltham, MA) for 30 min at 37°C, and observed using a confocal microscope (LSM800, Carl Zeiss Microscopy Ltd.,

Cambridge, MA). Images for analyzing ER/mitochondrial co-localization were acquired using 3D-deconvoluted stacks with the Z-stack application. The Pearson correlation coefficient[32], a well-defined and commonly accepted means for describing the extent of overlap between image pairs, was applied to quantify the degree of co-localization between the fluorophores representing DsRed2-ER and MitoTracker Green. The Pearson's correlation coefficient was analyzed using the built-in Carl Zeiss colocalization analysis module from the *ZEN* software, using the thresholding obtained from single-label control samples.

Mitochondrial Ca^{2+} Measurement

Mitochondrial Ca^{2+} levels in living cells were measured with a mitochondrial Ca^{2+} indicator, mitochondria-targeted ratiometric pericam (RPmt) (Ex. 418 nm and 494 nm, Em. 511 nm).[33, 34] Mouse neonatal cardiomyocytes were infected with an adenovirus encoding RPmt for 48 h at a multiplicity of infection (MOI) of 50. In adult cardiac myocytes, adenovirus-mediated RPmt gene transfer was performed 2 h after cell plating and at an MOI of 50. The experiments in adult cardiomyocytes were conducted 2 days after gene transfer. RPmt signals were collected by flow cytometry (FACScanto II flow cytometer; BD Bioscience, San Jose, CA) or observed using a confocal microscope (LSM800, Carl Zeiss Microscopy Ltd., Cambridge, MA). Quantitative analysis of flow cytometry data was determined using *FlowJo* (v10) software. The excitation ratio of RPmt confocal images was calculated by *MetaMorph* software (Molecular Devices, LLC. San Jose, CA).

Mitochondrial Ca^{2+} levels in mouse neonatal cardiomyocytes and adult cardiomyocytes were also measured with Rhod-2 probe (Ex/Em 552/581 nm, #R1245MP, Thermo Fisher Scientific, Waltham, MA). Stock solution (5 mM) was prepared in DMSO. Cells were incubated with Rhod-2 at the concentration of 5 μM for 30 min at 37°C. Cells were then washed to remove excess probe that either has not been loaded or may be noncovalently associated with the membrane. Rhod-2 signal were collected by flow cytometry (FACScanto II flow cytometer; BD Bioscience, San Jose, CA) or observed using a confocal microscope (LSM800, Carl Zeiss Microscopy Ltd., Cambridge, MA). Rhod-2 density was calculated by *ZEN* software (Zeiss).). Quantitative analysis of flow cytometry data was determined using *FlowJo* (v10) software. The quantification of Rhod-2 signals in confocal images was calculated by confocal build-in *Zen* software. MitoTracker® Green FM or MitoTracker™ Deeper Red FM (250 nm, Ex/Em 490/516 nm; #M22426, Thermo Fisher Scientific Inc. Waltham, MA) was used to co-stain cells for mitochondrial Ca^{2+}. The only MitoTracker positive areas were taken into Rhod-2 signal quantification in confocal pictures.

Assays of Mitochondrial Depolarization

Adult cardiac myocytes were loaded with TMRM probe (indicating $\Delta\Psi_m$) for 30 min at 37°C. Following incubation with the TMRM probe, cells were washed with PBS to remove free TMRM that either had not been loaded or was not associated with the membrane. Ru360 (10 μmol/L) was preloaded to the cells for 1 h at 37°C before measurement. The TMRM signals after histamine (100 μmol/L) stimulation was collected by time-lapse confocal microscopy (LSM800, Carl Zeiss Microscopy Ltd., Cambridge, MA). The

mitochondrial depolarization time represents the time of $\Delta\Psi_m$ reaching the lowest value minus the time at which the $\Delta\Psi_m$ begins to decrease.

Assays of Mitochondrial Permeability Transition Pore (MPTP)

MPTP in cardiomyocytes was assayed by using calcein-Co^{2+}, as described previously.[35] cardiomyocytes were loaded with 1 mmol/L calcein AM (Ex/Em 494/517 nm) for 30 min at 37°C in normal culture medium. When quenching of cytosolic and nuclear calcein fluorescence was required, 1 mmol/L $CoCl_2$ was present during calcein loading. After the attainment of quenching, cells were washed free of calcein and Co^{2+}, and calcein signal was monitored by confocal microscopy (LSM800, Carl Zeiss Microscopy Ltd., Cambridge, MA). If necessary, cyclosporine A (CsA, 1 μmol/L) or Ru360 (10 μmol/L) was added to the cells after calcein and Co^{2+} loading and 30 min before experimental recording.

Transmission Electron Microscopy (TEM)

Hearts from the indicated genotypes were first perfused with Ringer's solution (pH 7.4) to remove the blood and then perfused with fixative (4% paraformaldehyde, 1% glutaraldehyde in 0.1 mol/L sodium cacodylate buffer, pH 7.4, and 4% sucrose) to prefix the hearts. Next, the left ventricles were removed and post-fixed in a mixture of 0.8% potassium ferrocyanide and 2% osmium tetroxide in a 0.1 mol/L sodium cacodylate buffer for 2 h. After dehydration in a graded series of acetone, the samples were embedded in spurr resin and sectioned with a glass knife on a Leica Ultracut R cutter. The sections were stained with uranyl acetate and lead citrate, and observed using a Hitachi H-7600 TEM (Hitachi High-Technologies Europe GmbH, Krefeld, Germany).

Cultured H9c2 myoblasts were fixed with 2.5% glutaraldehyde in 0.1 mol/L sodium cacodylate buffer for 1 h at room temperature (RT). Cells were harvested with a cell scraper, and the aggregates were post-fixed with 1% osmium tetroxide in 0.1 mol/L cacodylate buffer for 1 h at RT, dehydrated in ethanol, and embedded in Epon 812 embedding resin. After polymerization, the plastic was removed and ultrathin sections were cut parallel and perpendicular to the flask surface. Thin sections were counterstained with uranyl acetate and lead nitrate, and examined with a Hitachi H-7600 TEM (Hitachi High-Technologies Europe GmbH, Krefeld, Germany).

The ER mitochondrial contacts were quantified as described previously.[18] The images were analyzed using ImageJ (National Institutes of Health). The mitochondrial and ER membranes were delineated using the freehand tool. The selected areas were converted to masks and perimeter of ER were calculated. Two independent investigators quantified the images blindly. For the MAM quantification, we normalized the total ER connected to mitochondria to total ER perimeter.

Oxygen Consumption Rate (OCR)

OCR was measured using an XF^e96 extracellular flux analyzer (Seahorse Biosciences, North Billerica, MA). Briefly, mouse neonatal cardiomyocytes were seeded in a 96-well plate ($^{\#}$102416-100, Seahorse Biosciences, North Billerica, MA) in the normal culture medium, followed by siRNA or adenovirus treatment for 48 h. The proper cell seeding

density was screened to make the control groups at the cell density of ~30K/well at the time of measurement. One hour before measurements, cells were removed from the CO_2 incubator and incubated at 37°C in a normal atmosphere. The medium was replaced with 180 μL XF assay medium (#102365-100, Seahorse Biosciences, North Billerica, MA) containing 10 mmol/L glucose, 1 mmol/L pyruvate, and 2 mmol/L glutamine at pH 7.4. Stock solutions of oligomycin, trifluoromethoxy carbonyl cyanide phenylhydrazone (FCCP), and rotenone/antimycin A in an XF Cell Mito Stress Test Kit (#103015-100, Seahorse Biosciences, North Billerica, MA) were prepared in XF assay medium and loaded into injection ports A, B, and C, respectively. The working concentrations for each inhibitor were as follows: Oligomycin 1 μmol/L, FCCP 4 μmol/L, Rotenone 0.5 μmol/L, and antimycin A 0.5 μmol/L. FCCP titration assay was applied to determine the optimal FCCP dosage by continuously injecting FCCP until the decreased OCR value was reached in mouse neonatal cardiomyocytes (data not shown). Measurements were obtained at 37°C. Assay cycles included 3 min of mixing, 2 min of a waiting period, and 3 min of measurement. The *Wave* software provided by Seahorse Biosciences was used for data collection. Basal respiration, maximal respiration, proton leak, coupled respiration, etc. were determined using the *XF Cell Mito Stress Test Generator* software provided by Seahorse Bioscience (North Billerica, MA). Coupling Assays were performed in isolated mitochondria from adult mouse hearts according to the published protocol.[36]

Detection of Reactive Oxygen Species (ROS)

Mitochondrial ROS levels were measured using MitoSOX™ Red (5 μmol/L Ex/Em 510/580 nm, #M36008, Thermo Fisher Scientific Inc., Waltham, MA). Mitochondrial membrane potential ($\Delta\Psi_m$) was measured with fluorescent probe rhodamine 123 (Rh123) (5 μmol/L Ex/Em 488/535 nm, #R8004, Sigma-Aldrich, St. Louis, MO) or TMRM (100 nmol/L Ex/Em 510/580 nm, #T668, Thermo Fisher Scientific Inc., Waltham, MA). Briefly, neonatal cardiomyocytes were incubated with each probe for 30 min at 37°C. Following incubation with the respective probes, cells were washed with PBS to remove free MitoSOX, or excess Rh123 and TMRM that either had not been loaded or was not associated with the membrane. When it was necessary, CsA (1 μmol/L) or Ru360 (10 μmol/L) was preloaded to the cells for 1 h at 37°C before measurement. Cells were then trypsinized with 0.25% trypsin and collected. The levels of mitochondrial MitoSOX, Rh123, and TMRM were measured by flow cytometer (FACScanto II; BD Bioscience, San Jose, CA). A minimum of 10,000 events was collected for each sample. Quantitative analysis of the data was determined using *FlowJo* (v10) software.

Detection of Apoptosis

Cell apoptosis in mouse neonatal cardiomyocytes were examined by Annexin V-FITC/PI Apoptosis Detection Kit (#556547, BD Bioscience, San Jose, CA). Cells were seeded to a 6-well plate. Twelve hours after incubation, cells were received NG (5.5 mmol/L) or HG (30 mmol/L) treatment for 48 h. CsA (1 μmol/L) or Ru360 (10 μmol/L) was preloaded to the cells for 1 h at 37°C before measurement. Cells were then washed with PBS and detached by trypsin followed by neutralization with culture medium. The detached cells were collected into a 15-mL centrifuged tube, and prepared according to manufacturer's instructions. The

apoptotic cell population was analyzed by a flow cytometer (FACScanto II; BD Bioscience, San Jose, CA).

Histology and Immunochemistry

Sirius Red staining was performed in heart paraffin section of the left ventricle using a Picro-Sirius Red Stain Kit (#ab150681, Abcam, Cambridge, MA). Terminal deoxynucleotidyl transferase dUTP nick end labeling (TUNEL) staining was performed in heart frozen section of the left ventricle using an *In Situ* Cell Death Detection Kit (Roche, Indianapolis, IN)

Reverse Transcription Polymerase Chain Reaction (RT-PCR)

Total RNA was isolated from cardiomyocytes or hearts using an RNeasy Mini Kit (#74106, QIAGEN N.V., Germany) and reverse-transcribed by iScript™ cDNA Synthesis Kit (#170-8891, Bio-Rad Laboratories, Inc. Hercules, CA). RT-PCR was performed using iQ™ SYBR® Green Supermix (#720001059, Bio-Rad Laboratories, Hercules, CA) in the CFX96™ Real-Time System (Bio-Rad Laboratories, Hercules, CA). Primer sequences for mouse *Fundc1*, *Itpr2*, and *Gadph* were shown as follows (5'-3'): *Fundc1* (F) CCCCCTCCCCAAGACTATGA; (R) CCACCCATTACAATCTGAGT; *Itpr2* (F) CCTCTACATTGGGGACATCGT; (R) GGCACACCTTGAACAGGCA; *Gadph* (F) CTACCCCACGGCAAGTTCA, (R) CCAGTAGACTCCACGACAAC.

Statistics

All data are expressed as means ± standard deviation (SD). All experiments were performed at least in triplicate, unless otherwise stated. Homogeneity of the variance was assessed using the F test (two groups) or the Brown-Forsythe test (≥ three groups). Normality of the data was assessed with the Shapiro-Wilk test. When reporting results with two groups, we used a standard Student's *t* test when the assumptions (equal variance and normal distribution) were satisfied. Otherwise, the non-parametric Mann-Whitney *U* test was used to analyze the difference between the two groups.

For results with more than two groups, analysis of variance (ANOVA) or other appropriate non-parametric tests was used to analyze the difference. When one variable was involved, we used a one-way ANOVA followed by the Bonferroni *post hoc* test when the assumptions (equal variance and normal distribution) were satisfied. Otherwise, we used the non-parametric Kruskal-Wallis test followed by Dunn's *post hoc* test to correct for multiple comparisons. For results with two variables, a two-way ANOVA followed by Bonferroni *post hoc* test was used for multiple comparisons when the assumptions (equal variances and normal distribution) were satisfied. Otherwise, we used the non-parametric Scheirer-Ray-Hare test (an extension of the Kruskal-Wallis test) followed by Dunn's *post hoc* test to correct for multiple comparisons.

P values were adjusted for multiple comparisons, where appropriate. *P* values < 0.05 were considered statistically significant. All statistical analyses were carried out using SPSS Version 21 software.

Results

Fundc1 Expression and MAM Formation are Increased in Diabetic Hearts

To determine the impact of diabetes on MAMs, we first examined the levels of MAM-related proteins in the hearts of STZ-treated diabetic mice. As shown in Supplemental Figures 1A and 1B, the levels of MAM-related proteins, including Fundc1, Ip_3r2, phosphofurin acidic cluster sorting protein 2 (Pacs-2), and Vdac1, were significantly higher ($P < 0.05$) in diabetic heart homogenates than in the non-diabetic counterparts. The levels of three other MAM-related proteins, sigma-1 receptor (Sig1r), Mfn2, and glucose-regulated protein 75 (Grp75), were comparable between control and diabetic hearts (Supplemental Figures 1A and 1B). In contrast, the levels of protein disulfide isomerase (Pdi) were decreased in STZ-treated hearts compared to non-diabetic counterparts (Supplemental Figures 1A and 1B). Notably, a higher level of beta-isoform of myosin heavy chain (β-Mhc) was observed in STZ-treated hearts than in non-diabetic counterparts (Supplemental Figures 1A and 1B), indicating cardiac hypertrophy in diabetic mice.

We then measured the MAM-related proteins in MAM fraction isolated from mouse hearts. The purity of the MAM fraction was demonstrated in Supplemental Figure 1C. Similar to the finding with heart homogenates, increased levels of both Fundc1 and Ip_3r2 were also detected in MAM fractions isolated from cardiac tissues of STZ-treated mice (Figure 1A). However, Pacs-2, Sig1r, Pdi, Grp75, and Vdac1 levels were unchanged in MAM fractions isolated from cardiac tissues of STZ-treated mice (Supplemental Figures 1D and 1E). To further establish that the observed effects were not due to off-target effects of STZ, a mitochondrial toxin, we examined MAM-related proteins in genetic diabetic Akita mice. Compared to those in WT groups, we found increased levels of both Fundc1 and Ip_3r2 in both cardiac homogenates (Supplemental Figures 2A and 2B) and cardiac MAM fractions (Figure 1B, Supplemental Figures 2C and 2D) in Akita mice.

To establish clinical relevance, we also examined FUNDC1 protein expression in the cardiac left ventricular tissues collected from human diabetic patients and non-diabetic donors (Supplemental Table 1). As depicted in Figure 1C, FUNDC1 levels were significantly elevated in cardiac tissues from diabetic patients compared to those in non-diabetic donors, thus confirming that FUNDC1 protein expression is increased in diabetic human hearts.

Next, we assessed MAM formation in diabetic murine hearts by analyzing the apposition of the ER and mitochondria. As illustrated by TEM images (Figure 1D), the association of the ER with mitochondria was dramatically increased in the hearts of diabetic Akita mice. Quantitative analysis indicated that the proportion of the ER adjacent to mitochondria was significantly increased in Akita mouse hearts (Figure 1E).

Hyperglycemia Promotes MAM Formation and Mitochondrial Ca^{2+} Increase in Cardiomyocytes

Hyperglycemia is a key pathological factor in type 1 diabetes. To explore the impact of HG on MAM formation, we evaluated the level of MAM-related proteins in mouse neonatal cardiomyocytes that received normal glucose (NG; 5.5 mmol/L D-glucose), osmotic control (5.5 mmol/L D-glucose plus 24.5 mmol/L D-mannitol), or HG (30 mmol/L D-glucose)

treatment. As depicted in Figures 2A and 2B, Supplemental Figures 3A and 3B, the levels of Fundc1, Ip_3r2, Pacs-2, and Vdac1 were significantly increased in HG-treated cells. We found no change in the levels of Pdi, Sig1r, Mfn2, or Grp75 (Supplemental Figures 3A and 3B). The value of Pearson's coefficient based on confocal imaging was applied to evaluate the association between ER and mitochondria. Consistently, confocal imaging (Figure 2C) and Pearson's correlation coefficient analysis (Figure 2D) revealed an increased association between the ER and mitochondria in HG-treated cells, but not in cells exposed to NG. Together, these data suggest that HG increases MAM formation in cardiomyocytes.

Next, we examined if HG-induced MAM formation was reversible. Forty-eight hours after HG treatment, HG medium was replaced with NG medium. MAMs were monitored in cardiomyocytes using live-cell time-lapse confocal microscopy. As depicted in Figures 2E and 2F, Eight hours after HG removal, HG-enhanced MAMs in cardiomyocytes were disassembled, and the number of MAMs returned to normal.

MAMs can transfer Ca^{2+} from the ER Ca^{2+} store into mitochondria. Therefore, we determined if increased diabetic MAM formation could result in mitochondrial Ca^{2+} increase. To this end, the mitochondrial Ca^{2+} indicator, RPmt (Figures 2G and 2H) was used to determine mitochondrial Ca^{2+} levels based on FCM analysis[37, 38]. As shown in Figures 2I and 2J, mitochondrial Ca^{2+} levels increased upon exposure to HG. Eight hours after the replacement of HG medium with NG medium, mitochondrial Ca^{2+} returned to basal levels (Figures 2I and 2J).

RPmt indicator is reported to sensitive to pH changes[39]. To further confirm if HG altered mitochondrial Ca^{2+}, we used Rhod-2 to detect mitochondrial Ca^{2+}. Considering Rhod-2 also distributes with non-mitochondrial compartments within a cell[40], we therefore used MitoTracker to co-stain mitochondria and used MitoTracker/Rhod-2- dual positive areas to calculate mitochondrial Ca^{2+} under confocal pictures. The mitochondrial membrane potential ($\Delta\Psi_m$) was simultaneously monitored under the same conditions. As depicted in Supplemental Figures 4A and 4B, $\Delta\Psi_m$ declined upon exposure to HG, while mitochondrial Ca^{2+} levels increased. Forty-eight hours after the replacement of HG medium with NG medium, both mitochondrial Ca^{2+} and $\Delta\Psi_m$ returned to basal levels.

$\Delta\Psi_m$ is directly related to the opening of MPTP. To determine if increased Ca^{2+} levels in diabetic conditions were pathological relevant, the calcein-Co^{2+} technique was used to measure the opening of MPTP in cells exposed to NG, HG, HG plus CsA (a specific inhibitor of MPTP), or HG plus Ru360 (a mitochondrial Ca^{2+} uptake inhibitor). As depicted in Supplemental Figures 5A and 5B, HG markedly reduced calcein signal in H9c2 rat myoblasts, which indicates HG induces long-time opening of MPTP. Moreover, HG-reduced calcein signal was largely inhibited by CsA/Ru360 addition (Supplemental Figures 5A and 5B), indicating that HG induces MPTP opening via promoting mitochondrial Ca^{2+} uptake. On the other hand, HG decreased $\Delta\Psi_m$ in mouse neonatal cardiomyocytes, which was prevented by the addition of CsA/Ru360 (Figure 2K).

Next, we evaluated apoptosis, the main consequence of the opening of MPTP in cardiomyocytes. As shown in Supplemental Figures 5C and 5D, HG induced cell apoptosis

in mouse neonatal cardiomyocytes and CsA/Ru360 ablated HG-induced apoptosis. Taken together, our results demonstrate that HG impairs mitochondrial function, induces MPTP opening, and triggers cell apoptosis by promoting mitochondrial Ca^{2+} uptake.

Overexpression of *Fundc1* Promotes MAM Formation, Mitochondrial Ca^{2+} Increase, and Mitochondrial Dysfunction in Cardiomyocytes

Since diabetes or HG causes aberrant *Fundc1* expression, we examined the impact of *Fundc1* overexpression on cardiomyocytes. Mouse neonatal cardiomyocytes were infected with *LacZ*- (ad-β-Gal) or *Fundc1*-expressing adenoviruses (ad-Fundc1) and MAM formation and mitochondrial function were examined forty-eight hour after infection. *Fundc1* overexpression increased MAM formation, as revealed by elevated levels of MAM-related proteins (Figure 3A, Supplemental Figures 6A and 6B) and increased ER-mitochondria contacts (Figures 3B and 3C). Consistently, *Fundc1* overexpression enhanced the percentage of ER adjacent to mitochondria in H9c2 myoblasts (Figures 3D and 3E). Increased MAM formation was associated with impairment of mitochondrial function, including higher mitochondrial Ca^{2+} levels (RPmt indicator: Figures 3F and 3G; Rhod-2 probe: Supplemental Figures 6C and 6D), mitochondrial ROS overproduction (Figure 3H), and decreased mitochondrial membrane potential (Figure 3I). We also measured OCR at the optimal cell density (30K cells/well) and FCCP concentration (1 μmol/L). We found that *Fundc1* overexpression reduced the OCR, including maximal respiration and spare respiratory capacity (Figure 3J). Taken together, these results suggest that upregulation of Fundc1 is involved in the development of diabetic cardiomyopathy.

Fundc1 is Required for ER-Mitochondria Contacts in Diabetic Hearts

To determine whether Fundc1 mediates MAM formation under diabetic conditions, we first compared the levels of MAM-related proteins in WT and *Fundc1* KO hearts of mice treated with vehicle or STZ. We found that STZ-induced diabetes increased Ip_3r2 in WT, but not in *Fundc1* KO hearts (Figure 4A). We then generated *Fundc1* KO Akita mice (Figure 4B). Similarly, compared with WT hearts, protein levels of Ip_3r2 were significantly increased in diabetic Akita hearts (Figure 4C). Importantly, the increase of Ip_3r2 was inhibited in *Fundc1* KO Akita hearts (Figure 4C).

Next, we assessed the effects of *Fundc1* deletion on MAM formation in Akita hearts by analyzing the apposition of ER and mitochondria in cardiomyocytes. As illustrated by TEM images (Figure 4D), *Fundc1* deletion reduced the association between the ER and mitochondria. In contrast, this association was dramatically increased in Akita hearts (Figure 4D) and the increased association was prevented by *Fundc1* deletion (Figure 4D). Quantitative analysis indicated that the proportion of the ER adjacent to mitochondria was significantly increased in Akita hearts, and this increase was abolished by deletion of *Fundc1* (Figure 4E). Therefore, these results demonstrate that Fundc1 contributes to the diabetes-induced cardiac ER-mitochondrial association.

We further validated our hypothesis in cultured mouse neonatal cardiomyocytes. Consistent with our findings above, HG treatment increased Ip_3r2 levels in WT cells, whereas there was no effect in *Fundc1* KO cells (Supplemental Figure 7A). TEM analysis indicated that

Fundc1 ablation reduced the proportion of ER adjacent to mitochondria in HG-treated cells (Supplemental Figures 7B and 7C). Confocal microscopic images also showed that HG increased ER-mitochondria contacts, and this increase was abolished by deletion of *Fundc1* (Supplemental Figures 7D and 7E), indicating that Fundc1 is required for diabetes-induced MAM formation.

Disrupting MAMs by Cardiac *Fundc1* Ablation Prevents Mitochondrial Ca^{2+} Increase, ROS Overproduction, and Mitochondrial Dysfunction in Diabetic Hearts

Given the fact that diabetes increases *Fundc1* expression in heart and Fundc1 is required for MAM formation in cardiomyocytes[11], we hypothesized that increases in the Fundc1-MAM axis could cause mitochondrial Ca^{2+} increase and mitochondrial dysfunction. To evaluate this hypothesis, we measured mitochondrial Ca^{2+} uptake using RPmt in adult mouse cardiomyocytes isolated from cardiac-specific *Fundc1* KO Akita mice. As depicted in Figures 5A and 5B, mitochondrial Ca^{2+} uptake was higher in Akita hearts than in WT hearts. Importantly, *Fundc1* KO inhibited mitochondrial Ca^{2+} uptake in Akita hearts (Figures 5A and 5B). Mitochondrial Ca^{2+} measured by Rhod-2 also supported that mitochondrial Ca^{2+} uptake was increased in Akita hearts compared with WT hearts (Supplemental Figure 8A**).** Consistently, *Fundc1* KO inhibited mitochondrial Ca^{2+} uptake in Akita hearts (Supplemental Figure 8A).

To explore if diabetic Ca^{2+} uptake was correlated with mitochondrial dysfunction, we measured $\Delta\Psi_m$ in adult cardiomyocytes from WT, *Fundc1* KO, Akita, and *Fundc1* KO Akita hearts before and after histamine stimulation. As depicted in Figures 5C and 5D, histamine induced a quicker mitochondrial depolarization in Akita cells than in WT cells. Ru360, which is a specific inhibitor of mitochondrial Ca^{2+} uptake, prevented $\Delta\Psi_m$ collapse in Akita cells after histamine stimulation (Figure 5C), indicating hyperglycemia induces mitochondrial depolarization by promoting mitochondrial Ca^{2+} uptake. *Fundc1* KO and *Fundc1* KO Akita cells protected against histamine-induced mitochondrial depolarization (Figure 5C). Importantly, histamine-induced mitochondrial Ca^{2+} uptake occurred 10 seconds prior to $\Delta\Psi_m$ decline, indicating that (1) $\Delta\Psi_m$ is required for Ca^{2+} uptake and (2) Ca^{2+} increase can cause $\Delta\Psi_m$ collapse, i.e., depolarization. The resting mitochondrial Ca^{2+} levels were higher in Akita hearts than that in WT hearts (Figure 5E). *Fundc1* KO Akita heart and *Fundc1* KO heart had lower levels of mitochondrial Ca^{2+} than that in WT hearts (Figure 5E). Mitochondrial Ca^{2+} assayed with Rhod-2 confirmed that increased levels of mitochondrial Ca^{2+} concentrations were found in diabetic Akita hearts (Supplemental Figures 8B and 8C). Moreover, the increase of mitochondrial Ca^{2+} concentrations was absent in *Fundc1* KO Akita mice (Supplemental Figures 8B and 8C).

Next, we assayed mitochondrial ROS levels and membrane potential in mitochondria isolated from adult WT, *Fundc1* KO, Akita, and *Fundc1* KO Akita mouse hearts by FCM. The purity of isolated mitochondria reached 85%, as evaluated by MitoTracker Green staining (Supplemental Figure 9A). The activity of isolated mitochondria reached 80%, as evaluated by MitoTracker Green and TMRM double staining (Supplemental Figure 9B). Mitochondrial Ca^{2+} increase, which impairs mitochondrial function, leading to reduced ATP production and increased release of ROS, is a key determinant in heart failure.[41] As

expected, both aberrant ROS production (Figures 5F and 5G) and reduced mitochondrial membrane potential (Figures 5H and 5I) were observed in diabetic Akita hearts. Importantly, we observed significantly improved mitochondrial membrane potential (Figures 5H and 5I) and less ROS production (Figures 5F and 5G) in *Fundc1* KO Akita hearts when compared to those in Akita mice.

Next, we used OCR to evaluate mitochondrial respiration capacity in mitochondria isolated from adult mouse hearts. As depicted in Figures 5J and 5K, the decreased OCR in state 3 and state 3u in Akita mitochondria was largely rescued by *Fundc1* deletion. Taken together, these results suggest that *Fundc1* deletion ablates impaired mitochondrial function driven by diabetes.

Cardiac *Fundc1* Ablation Alleviates Diabetic Cardiomyopathy *in vivo*

To establish the role of *Fundc1* in diabetic cardiomyopathy, we induced diabetes in WT and cardiomyocyte-specific *Fundc1* KO mice by STZ treatment and assayed cardiac function by echocardiography at 6 months. In WT mice, STZ-induced diabetes impaired cardiac function, revealed by significant increases in LVID (Table 1, Supplemental Figure 10A), significant decreases in EF (Table 1), FS (Table 1), and E/A ratio (Table 1, Supplemental Figure 10B), as well as increased IVRT (Table 1). These changes were accompanied by increased cardiac fibrosis (Supplemental Figures 10C and 10D). Intriguingly, compared with WT mice, *Fundc1* KO mice displayed increased in LVID (Table 1, Supplemental Figure 10A), decreased EF (Table 1) and FS (Table 1), reduced E/A ratio (Table 1, Supplemental Figure 10B), increased IVRT (Table 1), and increased cardiac fibrosis (Supplemental Figures 10C and 10D). However, cardiac-specific deletion of *Fundc1* almost completely prevented the cardiac abnormalities in STZ-treated diabetic mice, completely restoring LVID, EF, FS, E/A ratio, and IVRT to normal (Table 1, Supplemental Figures 10A and 10B). Cardiac fibrosis was also reduced in STZ-treated diabetic *Fundc1* KO mice, compared with diabetic WT mice (Supplemental Figures 10C and 10D). Additionally, the ratio of heart weight to tibia length was significantly increased in STZ-treated diabetic mice at 6 months, an effect that was completely prevented by *Fundc1* KO (Supplemental Figure 10E). Cardiomyocyte apoptosis, assayed by TUNEL staining, was markedly reduced in STZ-treated diabetic *Fundc1* KO mice when compared to diabetic WT mice (Supplemental Figures 10F and 10G).

We further verified the results observed in STZ-treated diabetic mice in cardiomyocyte-specific *Fundc1* KO Akita mice using echocardiography. Six-month-old *Fundc1* KO Akita mice did not display diabetes-induced cardiac abnormalities, evidenced by restored IVRT (Table 2, Supplemental Figure 10H). Finally, *Fundc1* deletion in Akita mice ablated the expression of pro-inflammatory cytokines, interleukin 6 (Il-6) and tumor necrosis factor alpha (Tnf-α), seen in Akita diabetic mice at 6 months (Supplemental Figures 10I and 10J). Taken together, our results suggested that Fundc1 plays a key role in the pathogenesis of diabetic cardiomyopathy.

Fundc1 Inhibits Ip_3r2 Ubiquitination and Proteasomal Degradation

Our previous study reported that Fundc1 is associated with the ER protein Ip_3r2 in heart homogenates[11]. Therefore, we evaluated if diabetes could promote binding of Fundc1 and Ip_3r2 in diabetic hearts. As depicted in Figure 6A, Akita hearts showed increased co-immunoprecipitation of Fundc1 and Ip_3r2, supporting the increased formation of MAMs under diabetic conditions. Further, immunofluorescence analysis confirmed Fundc1 and Ip_3r2 association in mouse neonatal cardiomyocytes (Supplemental Figure 11A).

The *Fundc1* and *Itpr2* mRNA levels were unchanged in diabetic hearts (Figure 6B) and HG-treated neonatal cardiomyocytes (Supplemental Figure 11B). Next, we determined if *Fundc1* overexpression in mouse neonatal cardiomyocytes could alter *Itpr2* mRNA levels. As shown in Figure 6C, adenovirus-mediated *Fundc1* overexpression had no effect on *Itpr2* mRNA expression, suggesting that Fundc1 may affect Ip_3r2 protein levels by regulating its degradation. Thus, we examined if Fundc1 could alter ubiquitin and proteasome-mediated Ip_3r2 degradation. To this end, both *control* siRNA- and *Fundc1* siRNA-treated mouse neonatal cardiomyocytes were treated with the proteasome inhibitor MG132 (160 nmol/L) or lactacystin (40 nmol/L) for 48 h. Administration of either MG132 (Figure 6D) or lactacystin (Supplemental Figure 11C) abolished the reduction of Ip_3r2 induced by *Fundc1* silencing. In contrast, *Fundc1* overexpression inhibited Ip_3r2 ubiquitination and increased Ip_3r2 stability (Figure 6E). These data indicate Fundc1 inhibits Ip_3r2 ubiquitination and proteasome degradation.

Ring finger protein 170 (Rnf170) is an E3 ligase that mediates Ip_3r2 ubiquitination[42]. Therefore, we examined whether Fundc1 inhibits Ip_3r2 degradation by downregulating Rnf170. As depicted in Supplemental Figure 11D, protein levels of Rnf170 were comparable between WT and *Fundc1* KO hearts. Alternatively, we found that *Fundc1* deletion reduced the association between Ip_3r2 and Fundc1 (Figure 6F) with a concomitant increase of Ip_3r2 and Rnf170 interaction, as well as Ip_3r2 ubiquitination (Figure 6F). In *Fundc1* KO Akita hearts, there was an increased binding between Ip_3r2 and Rnf170, and increased Ip_3r2 ubiquitination (Figure 6F). Taken together, our data suggest that binding of Fundc1 to Ip_3r2 inhibits Ip_3r2 ubiquitination and proteasome-mediated degradation.

The N-terminal of Fundc1 is Required for Binding to Ip_3r2 and MAM Formation

To determine how Fundc1 interacts with Ip_3r2, we generated a mutant of Fundc1 by truncating amino acids 7-48, the N-terminal cytosolic domain of the Fundc1 protein. We found that this Fundc1 truncation (Fundc1Δ7-48) reduced the association between Ip_3r2 and Fundc1 (Figure 6G) with a concomitant increase of Ip_3r2 ubiquitination (Figure 6G), indicating that the Fundc1 binds Ip_3r2 with the cytosolic N-terminal domain. Using confocal microscopy, we further determined the subcellular location of Fundc1Δ7-48. As depicted in Figure 6H, Fundc1Δ7-48 co-localized with mitochondria; however, the truncated Fundc1 protein decreased contacts between ER and mitochondria (Figures 6H and 6I), suggesting that the Ip_3r2-binding domain of Fundc1 N-terminal is required for MAM formation.

Disrupting MAMs by *Itpr2* Silencing Prevents Hyperglycemia-driven Mitochondrial Ca^{2+} Increase and Mitochondrial Dysfunction in Cardiomyocytes

Since regulation of Ca^{2+} flux between the ER and mitochondria via Ip_3rs is a major function of MAMs[1], we asked whether diminishing ER-mitochondrial Ca^{2+} flux could improve mitochondrial function and reduce apoptotic cell death under diabetic conditions. To this end, we decreased ER-mitochondrial Ca^{2+} flux by suppressing Ip_3r2 in cardiomyocytes. As depicted in Supplemental Figures 12A and 12B, *Itpr2* silencing reduced the mitochondrial Ca^{2+} concentration under NG conditions and abolished the HG-induced mitochondrial Ca^{2+} increase. Similar results were obtained using Rhod-2: *Itpr2* silencing reduced the mitochondrial Ca^{2+} concentration under NG conditions and abolished HG-induced mitochondrial Ca^{2+} increases (Supplemental Figures 12C and 12D). In addition, *Itpr2* silencing coincided with a reduction of mitochondrial ROS production (Supplemental Figures 12E and 12F) and restoration of mitochondrial membrane potential (Supplemental Figures 12G and 12H). The restoration of mitochondrial Ca^{2+} homeostasis was associated with improved mitochondrial maximal oxidative capacity and spare respiratory capacity (Supplemental Figures 12I and 12J). These findings suggest that Ip_3r2-mediated ER-mitochondrial Ca^{2+} transport is critical for HG-induced mitochondrial dysfunction.

Diabetes Inhibits AMP-activated Protein Kinase (Ampk) in Hearts.

Ampkα2 is the predominant isoform of Ampk in cardiomyocytes, and decreased Ampkα2 activity is an important event in the development of diabetic cardiomyopathy[43]. Chronic Ampk activation by metformin prevents cardiomyopathy by restoring mitochondrial and cardiac ultrastructure in diabetic OVE26 mice[43]. Thus, we set out to evaluate whether Ampk reduction in diabetic hearts contributes to aberrant MAM formation. To this end, we monitored Ampk activity by measuring Ampk phosphorylation at Thr172 (pAmpk) in the cardiac muscle of vehicle- or STZ-treated mice. As depicted in Figures 7A and 7B, pAmpk was significantly decreased in STZ-treated hearts when compared with non-diabetic hearts. In contrast, the protein levels of Ampkα2 were comparable between vehicle- and STZ-treated hearts (Figures 7A and 7B). The reduction of pAmpk was concomitantly associated with an increase of Fundc1. Similarly, reduced levels of pAmpk, along with increased Fundc1, were also found in the hearts of Akita mice (Figures 7C and 7D).

Ampk Inhibition is Associated with Aberrant Fundc1 in Cardiomyocytes *in vitro* and *in vivo*

To determine if decreased Ampk activity promotes Fundc1 upregulation in the heart, we measured Fundc1 levels in WT and *Prkaa2* (gene of Ampkα2) KO mouse hearts. As shown in Figures 7E and 7F, the protein levels of Fundc1 were largely increased in *Prkaa2* KO hearts, compared with WT hearts. To explore whether increased Fundc1 in *Prkaa2* KO hearts was concomitant with enhanced MAM formation, we used confocal microscopy to determine the association between ER and mitochondria in WT and *Prkaa2* KO mouse neonatal cardiomyocytes. As depicted in Figures 7G and 7H, the association between the ER and mitochondria was significantly increased in *Prkaa2* KO cells compared with WT cells. As expected, the resting mitochondrial Ca^{2+} levels revealed by RPmt were higher in *Prkaa2* KO cells than in WT cells (Figures 7I and 7J; the plots for each channel are shown in Supplemental Figure 13A). Similarly, the resting mitochondrial Ca^{2+} levels detected by

Rhod-2 probe were elevated in *Prkaa2* KO cells when compared with WT cells (Supplemental Figures 13B and 13C).

To establish a causative link between reduced Ampk and increased Fundc1 in diabetic conditions, we monitored the levels of Ampk phosphorylation at Thr172 (pAmpk) and Fundc1 in mouse neonatal cardiomyocytes before HG, with HG, and after HG. Compared to cells cultured in NG, cells that received HG treatment had lower pAmpk levels, but higher Fundc1 and Ip_3r2 levels (Figures 7K and 7L). Interestingly, eight hours after HG removal, pAmpk, Fundc1 and Ip_3r2 returned to basal levels (Figures 7K and 7L).

Ampk Prevents HG-Induced Fundc1, MAMs, and Mitochondrial Ca^{2+} Increase in Cultured Mouse Neonatal Cardiomyocytes

To investigate if the HG conditions of type 1 diabetes increase Fundc1 via inhibition of Ampk activity *in vivo*, NG- or HG-treated mouse neonatal cardiomyocytes were infected with adenoviruses encoding β-Gal (ad-β-Gal) or constitutively active mutant Ampk (ad-Ampk-CA). As depicted in Figure 7M, Ampk activation following ad-Ampk-CA infection abolished HG-induced *Fundc1* expression. Further, Ampk activation inhibited HG-induced MAM formation (Figure 7N) and prevented HG-induced mitochondrial Ca^{2+} increase (Figure 7O; the plots for each channel are shown in Supplemental Figure 13D) and mitochondrial depolarization (Figure 7P). Similarly, mitochondrial Ca^{2+} assayed by Rhod-2 also supported that AMPK activation prevented HG-induced mitochondrial Ca^{2+} increase (Supplemental Figures 13E and 13F). Taken together, our results demonstrate that via downregulation of Ampk, HG increases Fundc1, Fundc1-mediated MAMs, and mitochondrial Ca^{2+} increase in diabetic hearts.

Discussion

In the present study, we have for the first time reported that diabetes-mediated MAM formation causes aberrant Ca^{2+} signaling, which in turn leads to diabetic mitochondrial dysfunction and cardiomyopathy (Supplemental Figure 14). Disrupting MAMs in cardiomyocytes by genetic deletion of *Fundc1* ablates mitochondrial Ca^{2+} increase, mitochondrial dysfunction, and cardiac dysfunction in diabetic mice. We found that Fundc1 interacts with Ip_3r2 and inhibits Ip_3r2 ubiquitination and proteasomal degradation. Additionally, *Prkaa2* KO mice display increased Fundc1 and mitochondrial Ca^{2+} increase. Continuous activation of Ampk in cardiomyocytes prevents HG-induced MAM formation, mitochondrial Ca^{2+} increase, and mitochondrial dysfunction. We therefore conclude that HG-induced Ampk inhibition causes diabetic cardiomyopathy by increasing Fundc1, Fundc1-related MAMs, and mitochondrial Ca^{2+} increase in the heart.

The most important finding of the present study is that diabetes-induced Fundc1 is involved in the pathogenesis of diabetic cardiomyopathy. Importantly, cardiac-specific deletion of *Fundc1* improves mitochondrial function and attenuates cardiomyopathy in diabetic mice, confirming the causative role of Fundc1 in this disorder. We have provided compelling evidence to demonstrate that Fundc1 is an important molecule that mediates diabetes-induced MAM formation and mitochondrial Ca^{2+} increase, a new mechanism for diabetic mitochondrial dysfunction. First, hyperglycemia increases MAM-associated Fundc1 levels,

which enhances Fundc1 binding to the ER protein Ip_3r2. This increases mitochondrial Ca^{2+} uptake, resulting in mitochondrial Ca^{2+} increase and mitochondrial dysfunction. Second, Fundc1 interacts with Ip_3r2, and inhibits Ip_3r2 ubiquitination and proteasomal degradation. Third, diabetes promotes association of the ER with mitochondria and increases the abundance of Ip_3r2 in MAMs. Fourth, genetic deletion of *Fundc1* decreases Ip_3r2 abundance and reduces mitochondrial-ER contacts. Fifth, Fundc1 controls diabetes-associated MAM function, resulting in mitochondrial Ca^{2+} increase and mitochondrial dysfunction. Finally, *Fundc1* overexpression in cardiomyocytes induces a diabetes-like phenotype, including increased MAM formation, mitochondrial Ca^{2+} increase, and mitochondrial dysfunction. These findings are in line with published data showing that diabetic cardiomyopathy is associated with abnormal mitochondrial structure and function, a central event in the pathogenesis of diabetic cardiomyopathy.[1]

Enhanced MAM formation under diverse pathological conditions[44] initiates mitochondrial Ca^{2+} increase, resulting in mitochondrial dysfunction. For example, decreasing mitochondria-reticulum interactions by deletion of CypD, an important molecule that interacts with the Vdac1-Ip_3r1 bridge, protects cardiomyocytes from lethal hypoxia-reoxygenation injury through the reduction of mitochondrial Ca^{2+} increase.[20] An important observation of the present study is that Fundc1 promotes Ca^{2+} increase and mitochondrial dysfunction via increased MAMs. Indeed, we found only two MAM-related proteins, Fundc1 and Ip_3r2, were increased in MAM fractions of diabetic hearts. More importantly, we observed an increased interaction between Fundc1 and Ip_3r2 in diabetic hearts. Our finding is consistent with a previous report that demonstrates the importance of MAMs for mitochondrial Ca^{2+} homeostasis[12].

We have for the first time unveiled a novel link between Ampk and MAMs in cardiomyocytes. In particular, Ampk appears to be a major regulator of MAMs, at least in the heart. In addition, deregulated Ampk contributes to diabetic cardiomyopathy by causing aberrant numbers of Fundc1-related MAMs. This is supported by the following evidence: 1) both MAM formation and mitochondrial Ca^{2+} levels were largely increased in *Prkaa2*-null hearts compared with WT hearts; 2) diabetic hearts had decreased Ampk activity and enhanced MAM formation compared with normal hearts; 3) continuous activation of Ampk in HG-treated cultured mouse neonatal cardiomyocytes inhibited MAM formation and mitochondrial Ca^{2+} increase. Of interest, metformin, one of the most commonly used anti-diabetic drugs for type 2 diabetes is a well-characterized Ampk activator[43, 45-47]. Activation of Ampk by metformin improves cardiac function and reduces the incidence of myocardial infarction in diabetic obese patients according to the UK Prospective Diabetes Study.[48] Our previous study demonstrated that metformin-induced chronic Ampk activation prevents cardiomyopathy by recovering mitochondrial and cardiac ultrastructure in diabetic OVE26 mice[43]. The present study offers evidence supporting the concept that metformin, used exclusively for type 2 diabetes, might be a useful tool for treating diabetic cardiomyopathy in type 1 diabetes. Larger trials are warranted to evaluate the potential effects of metformin in cardiovascular outcomes in patients with type 1 diabetes.

Precise control of mitochondrial fission and fusion is essential to maintain normal cardiac function because both excessive fusion and fission have been shown to be deleterious to the

heart. For example, cardiac-specific *Dnm1L* (the gene encoding Drp1) KO mice developed left ventricular dysfunction, which was preceded by mitochondrial elongation and mitochondrial dysfunction.[49] Additionally, the deletion of cardiac *Mfn1* and *Mfn2* suppressed fusion and was concurrent with cardiac dysfunction.[50] In this study, we found that diabetes increased *mitochondrial fission 1 protein* (*Fis1*) expression, induced excess mitochondrial fission (Supplemental Figures 15 and 16), and impaired cardiac structure and function. Conversely, in *Fundc1* KO mice, *Fis1* expression was reduced, leading to excess mitochondrial fusion and cardiac dysfunction (Supplemental Figures 15 and 16).[11] Importantly, *Fundc1* deletion could restore normal mitochondrial morphology in diabetic cardiomyocytes via suppression of *Fis1* expression (Supplemental Figures 15 and 16), which resulted in improved cardiac structure and function.

Fundc1 levels are closely connected to the MAM levels in cardiomyocytes. The MAMs-localized Fundc1 binds to Ip_3r2 to mediate Ip_3rs-dependent Ca^{2+} release from ER into both mitochondria and cytosols in cardiomyocytes. *Fundc1* deletion in cardiomyocytes instigates cardiac dysfunction and heart failure by reducing mitochondrial Ca^{2+} levels and mitochondrial fission. Under diabetic conditions, however, abnormally increased levels of Fundc1 and Fundc1-related MAMs cause mitochondrial Ca^{2+} increase mediated by Fundc1-mediated MAMs. Mitochondrial Ca^{2+} increase impairs mitochondrial function in multiple ways, including mitochondrial fragmentation, deceased mitochondrial OCR, long-time MPTP opening, as well as cell apoptosis. Consistently, *Fundc1* deletion prevents HG-induced mitochondrial Ca^{2+} increase, mitochondrial fragmentation (Supplemental Figures 15 and 16), mitochondrial OCR reduction, long-time MPTP opening, and cell apoptosis. Thus, it is reasonable for us to conclude that *Fundc1* deletion improves/prevents diabetic cardiomyopathy by disrupting MAMs and MAMs-related mitochondrial Ca^{2+} increase in cardiomyopathy.

Fundc1 appears to be essential in maintaining normal cardiac functions but is increases in stress conditions such as insulin resistance or diabetes causes cardiac myopathy. Similar findings have been observed in diabetic hearts. For example, in the adult heart, the transcriptional factor forkhead box-1 (FoxO-1) is important in keeping cardiomyocytes in the homeostatic state.[51, 52] But in diabetes and insulin resistance status, FoxO-1, which becomes overproduced/over-activated in response to stress stimuli, triggers diabetic cardiomyopathy.[53, 54]

The Akita mouse is a well-validated, non-obese model of human type 1 diabetes, which is also free of the potential confounding effects of STZ administration.[55, 56] Both Akita mice and STZ-induced diabetic mice are commonly used experimental animal models for studying diabetic cardiomyopathy; however, they differ in some functional, structural, and metabolic abnormalities.[57, 58] Briefly, Akita mice have diastolic dysfunction with preserved systolic function, whereas STZ mice have both diastolic and systolic dysfunction.[57, 58] Akita mice do not have myocardial hypertrophy or fibrosis, whereas STZ diabetic mice have both.[57, 58] Our current findings are consistent with these earlier reports.[57, 58] The difference between these mouse models manifests in the different pattern of hyperglycemia induction: Akita mice have chronic and sustained increased blood glucose due to genetic manipulation, whereas STZ mice have an acute blood glucose increase due to STZ administration.

However, regardless of this difference, *Fundc1* KO attenuated abnormalities in both Akita and STZ hearts, which supports our major conclusion that *Fundc1* gene deletion can protect against diabetic cardiomyopathy.

Fundc1 can interact with Lc3 and act as a mitophagy receptor.[23, 24] Although diabetes markedly increases levels of Fundc1, we did not observe increased mitophagy under diabetic conditions (**data not shown**). Of note, the removal of damaged mitochondria by autophagy requires mitophagy receptor proteins, induction of general autophagy, and activation of the PTEN-induced putative kinase 1 (Pink1)-Parkin signaling pathway, to prime damaged mitochondria for selective autophagic recognition.[59] In diabetic hearts, autophagy is suppressed and Pink1 and Parkin protein levels are reduced, accompanied by decreased expression of the lysosomal-associated membrane protein 1 (Lamp1).[60] Thus, upregulation of Fundc1, a mitophagy receptor, is not sufficient to induce mitophagy under diabetic conditions. The defective mitophagy results in the accumulation of compromised mitochondria that release ROS and pro-apoptotic factors, resulting in impaired cardiac structure and function.

Mitochondrial Ca^{2+} signaling controls cell metabolism and cell death by necrosis, apoptosis, and autophagy.[61] For example, transient fluctuations in mitochondrial Ca^{2+} activate three matrix dehydrogenases (pyruvate dehydrogenase, α ketoglutarate- and isocitrate-dehydrogenases, and dehydrogenases) and oxidative phosphorylation, which stimulates ATP production.[62] Accordingly, deletion of all three *Ip3rs* diminishes mitochondrial Ca^{2+} uptake, leading to compromised mitochondrial function.[63] Further, mitochondrial Ca^{2+} increase is associated with apoptosis of cardiac cells in response to ischemia-reperfusion injury.[64, 65] These data suggest that maintaining a proper Ca^{2+} flux between the ER and mitochondria is essential for mitochondrial and metabolic homeostasis. Consistent with these findings, downregulation of key molecules involved in the ER-mitochondria association and Ca^{2+} flux, such as *Ip3r2*, improved mitochondrial respiration, inhibited oxidative stress, and reduced apoptotic cell death in cultured cardiomyocytes under HG growth conditions. Similar results were also observed in *Fundc1*-null cardiomyocytes, in which the contacts between the ER and mitochondria were disrupted. More importantly, cardiac-specific deletion of *Fundc1* attenuated mitochondrial dysfunction, cardiomyocyte apoptosis, and cardiac dysfunction in diabetic mice. These results support the importance of mitochondrial Ca^{2+} homeostasis in maintaining normal cardiac structure and function.

Mitochondrial Ca^{2+} uptake via MCU is in a $\Delta\Psi_m$-dependent way.[66] Excessively up-taken Ca^{2+} reduces $\Delta\Psi_m$ either directly by the entry of positive charge[67, 68] or indirectly by triggering long-time MPTP opening[65]. Mitochondrial Ca^{2+} uptake is followed by an NCLX-mediated mitochondrial Ca^{2+} extrusion (efflux) or so-called Ca^{2+} efflux. Mitochondrial Ca^{2+} stopped efflux or extrusion when $\Delta\Psi_m$ declined although how $\Delta\Psi_m$ collapse induces mitochondrial Ca^{2+} efflux remains unclear. In the heart and many other mammalian tissues, a putative Na^+/Ca^{2+} exchanger (NCLX) is the major pathway for Ca^{2+} efflux from the mitochondrial matrix.[69] Further, mitochondrial Ca^{2+} efflux after mitochondrial Ca^{2+} uptake is regulated by Ca^{2+} release channel NCLX.[70] In work by Palty et al., overexpression of NCLX enhances mitochondrial Ca^{2+} efflux while overexpression of inactive NCLX mutant inhibits mitochondrial Ca^{2+} efflux. It is of interest to note that in diabetic cardiomyocytes

high mitochondrial Ca^{2+} was found to be co-existed with low $\Delta\Psi_m$, which indicates that HG not only promotes mitochondrial Ca^{2+} uptake via enhanced MAM formation but also inhibits mitochondrial Ca^{2+} efflux. Our data are consistent with published observations that depolarized mitochondria maintain high mitochondrial Ca^{2+} after agonist stimulation.[71] Further, low $\Delta\Psi_m$ is found with elevated mitochondrial Ca^{2+} in palmate (PA)-treated H9c2 myoblasts.[72] Moreover, another report shows that the mitochondrial Ca^{2+} efflux after HG-induced mitochondrial Ca^{2+} uptake was largely inhibited by si*Slc8b1* (gene encoding NCLX) in primary beta cells.[73] How diabetes impairs mitochondrial Ca^{2+} efflux in cardiomyocytes warrants further investigation.

Precisely measuring mitochondrial Ca^{2+} is a very challenge task, as currently used probes have their limitations. In this study, two methods: RPmt[33, 34] and Rhod-2[74], were used for mitochondrial Ca^{2+} detection. The RPmt is a well-characterized mitochondrial Ca^{2+} indicator because of its exclusively mitochondrial localization and ratiometric property to avoid uneven loadings.[33, 34] However, the RPmt has been reported not only to sense the changes of Ca^{2+} but also pH.[39] Rhod-2 is also widely used for intercellular Ca^{2+} probe despite the main limitation of Rhod-2 probe is its non-mitochondrial loading (e.g., nucleus).[40, 75] To exclude the effect of off-targeting, we used MitoTracker to co-stain mitochondria and then quantified those Rhod-2/MitoTracker–co-stained signals under confocal microscope. Notably, the results obtained with RPmt and Rhod-2 were similar, which support the concept that diabetes might cause mitochondrial Ca^{2+} increase. Since there is no specific method for us to precisely measure mitochondrial pH, we cannot exclude the possibility that the RPmt signals we measured might come from mitochondrial pH changes. Although we consider it very unlikely, it remains possible that mitochondrial pH change might affect the intensities of both probes.

In summary, we have identified a new role for Fundc1 in mediating diabetes-induced MAM formation and in turn, mitochondrial Ca^{2+} increase. This mitochondrial Ca^{2+} increase impairs mitochondrial function, resulting in impairment of cardiac structure and function. Diabetes induces MAM formation, likely through downregulation of Ampk. Ampk activation, likely via downregulation of Fundc1 and Fundc1-related MAMs, represents a new therapeutic avenue for treating diabetic cardiomyopathy.

Supplementary Material

Refer to Web version on PubMed Central for supplementary material.

Acknowledgments

M.H.Z. and Z.X. conceived the project. M.H.Z., Z.X., and S.W. designed the study and wrote the manuscript. S.W. conducted confocal microscopy imaging, OCR measurements, FCM analysis, immunoprecipitation, and western blot. Q.L. conducted cardiac function measurements. Y.D. performed immunohistochemistry staining. X.M. and K.H. performed human studies. P.W. prepared the RPmt adenovirus. All authors have approved the manuscript. We thank Dr. Wang from the University of Washington for kindly providing the mitochondrial Ca^{2+} indicator PRmt.

Sources of Funding

This study was supported by funding from the following agencies: The National Heart, Lung, and Blood Institute (NHLBI) (HL079584, HL080499, HL089920, HL110488, HL128014, HL132500, HL137371, HL142287, and HL140954); The National Cancer Institute (NCI) (CA213022); The National Institute on Aging (NIA)

(AG047776); The American Heart Association (AHA) (16GRANT29590003). Dr. Zou is the Eminent Scholar in Molecular and Translational Medicine of Georgia Research Alliance. Dr. Wu was supported by an American Heart Association postdoctoral fellowship award (16POST29960011). Dr. Ding was supported by an American Heart Association postdoctoral fellowship award (16POST31160009).

References

1. Brownlee M Biochemistry and molecular cell biology of diabetic complications. Nature. 2001;414:813–820. doi: 10.1038/414813a. [PubMed: 11742414]
2. Green DR, Kroemer G. The pathophysiology of mitochondrial cell death. Science. 2004;305:626–629. doi: 10.1126/science.1099320. [PubMed: 15286356]
3. Patti ME, Corvera S. The role of mitochondria in the pathogenesis of type 2 diabetes. Endocr Rev. 2010;31:364–395. doi: 10.1210/er.2009-0027. [PubMed: 20156986]
4. Kelley DE, He J, Menshikova EV, Ritov VB. Dysfunction of mitochondria in human skeletal muscle in type 2 diabetes. Diabetes. 2002;51:2944–2950. doi: 10.2337/diabetes.51.10.2944. [PubMed: 12351431]
5. Zhang D, Liu ZX, Choi CS, Tian L, Kibbey R, Dong J, Cline GW, Wood PA, Shulman GI. Mitochondrial dysfunction due to long-chain Acyl-CoA dehydrogenase deficiency causes hepatic steatosis and hepatic insulin resistance. Proc Natl Acad Sci U S A. 2007;104:17075–17080. doi: 10.1073/pnas.0707060104. [PubMed: 17940018]
6. Lowell BB, Shulman GI. Mitochondrial dysfunction and type 2 diabetes. Science. 2005;307:384–387. doi: 10.1126/science.1104343. [PubMed: 15662004]
7. Giorgi C, De Stefani D, Bononi A, Rizzuto R, Pinton P. Structural and functional link between the mitochondrial network and the endoplasmic reticulum. Int J Biochem Cell Biol. 2009;41:1817–1827. doi: 10.1016/j.biocel.2009.04.010. [PubMed: 19389485]
8. Vance JE, Stone SJ, Faust JR. Abnormalities in mitochondria-associated membranes and phospholipid biosynthetic enzymes in the mnd/mnd mouse model of neuronal ceroid lipofuscinosis. Biochim Biophys Acta. 1997;1344:286–299. doi: 10.1016/S0005-2760(96)00153-1. [PubMed: 9059519]
9. Szabadkai G, Bianchi K, Varnai P, De Stefani D, Wieckowski MR, Cavagna D, Nagy AI, Balla T, Rizzuto R. Chaperone-mediated coupling of endoplasmic reticulum and mitochondrial Ca^{2+} channels. J Cell Biol. 2006;175:901–911. doi: 10.1083/jcb.200608073. [PubMed: 17178908]
10. de Brito OM, Scorrano L. Mitofusin 2 tethers endoplasmic reticulum to mitochondria. Nature. 2008;456:605–610. doi: 10.1038/nature07534. [PubMed: 19052620]
11. Wu S, Lu Q, Wang Q, Ding Y, Ma Z, Mao X, Huang K, Xie Z, Zou MH. Binding of FUNDC1 with inositol 1,4,5-trisphosphate receptor in mitochondria-associated endoplasmic reticulum (ER) membranes maintains mitochondrial dynamics and function in hearts in vivo. Circulation. 2017 136:2248–2266. doi: 10.1161/CIRCULATIONAHA.117.030235. [PubMed: 28942427]
12. Rowland AA, Voeltz GK. Endoplasmic reticulum-mitochondria contacts: function of the junction. Nat Rev Mol Cell Biol. 2012;13:607–625. doi: 10.1038/nrm3440. [PubMed: 22992592]
13. Del Prete D, Suski JM, Oules B, Debayle D, Gay AS, Lacas-Gervais S, Bussiere R, Bauer C, Pinton P, Paterlini-Brechot P, Wieckowski MR, Checler F, Chami M. Localization and processing of the amyloid-beta protein precursor in mitochondria-associated membranes. J Alzheimers Dis. 2017;55:1549–1570. doi: 10.3233/jad-160953. [PubMed: 27911326]
14. Danese A, Patergnani S, Bonora M, Wieckowski MR, Previati M, Giorgi C, Pinton P. Calcium regulates cell death in cancer: roles of the mitochondria and mitochondria-associated membranes (MAMs). Biochim Biophys Acta Bioenerg. 2017;1858:615–627. doi: 10.1016/j.bbabio.2017.01.003. [PubMed: 28087257]
15. Marchi S, Patergnani S, Pinton P. The endoplasmic reticulum-mitochondria connection: one touch, multiple functions. Biochim Biophys Acta. 2014;1837:461–469. doi: 10.1016/j.bbabio.2013.10.015. [PubMed: 24211533]
16. Betz C, Stracka D, Prescianotto-Baschong C, Frieden M, Demaurex N, Hall MN. Feature article: mTOR complex 2-Akt signaling at mitochondria-associated endoplasmic reticulum membranes (MAM) regulates mitochondrial physiology. Proc Natl Acad Sci U S A. 2013;110:12526–12534. doi: 10.1073/pnas.1302455110. [PubMed: 23852728]

17. Tubbs E, Theurey P, Vial G, Bendridi N, Bravard A, Chauvin MA, Ji-Cao J, Zoulim F, Bartosch B, Ovize M, Vidal H, Rieusset J. Mitochondria-associated endoplasmic reticulum membrane (MAM) integrity is required for insulin signaling and is implicated in hepatic insulin resistance. Diabetes. 2014;63:3279–3294. doi: 10.2337/db13-1751. [PubMed: 24947355]

18. Arruda AP, Pers BM, Parlakgul G, Guney E, Inouye K, Hotamisligil GS. Chronic enrichment of hepatic endoplasmic reticulum-mitochondria contact leads to mitochondrial dysfunction in obesity. Nat Med. 2014;20:1427–1435. doi: 10.1038/nm.3735. [PubMed: 25419710]

19. Di Lisa F, Canton M, Menabo R, Kaludercic N, Bernardi P. Mitochondria and cardioprotection. Heart Fail Rev. 2007;12:249–260. doi: 10.1007/s10741-007-9028-z. [PubMed: 17516167]

20. Paillard M, Tubbs E, Thiebaut PA, Gomez L, Fauconnier J, Da Silva CC, Teixeira G, Mewton N, Belaidi E, Durand A, Abrial M, Lacampagne A, Rieusset J, Ovize M. Depressing mitochondria-reticulum interactions protects cardiomyocytes from lethal hypoxia-reoxygenation injury. Circulation. 2013;128:1555–1565. doi: 10.1161/CIRCULATIONAHA.113.001225. [PubMed: 23983249]

21. Choi KM, Zhong Y, Hoit BD, Grupp IL, Hahn H, Dilly KW, Guatimosim S, Lederer WJ, Matlib MA. Defective intracellular Ca(2+) signaling contributes to cardiomyopathy in type 1 diabetic rats. Am J Physiol Heart Circ Physiol. 2002;283:H1398–H1408. doi: 10.1152/ajpheart.00313.2002. [PubMed: 12234790]

22. Pierce GN, Russell JC. Regulation of intracellular Ca^{2+} in the heart during diabetes. Cardiovasc Res. 1997;34:41–47. doi: 10.1016/S0008-6363(97)00010-2. [PubMed: 9217871]

23. Liu L, Feng D, Chen G, Chen M, Zheng Q, Song P, Ma Q, Zhu C, Wang R, Qi W, Huang L, Xue P, Li B, Wang X, Jin H, Wang J, Yang F, Liu P, Zhu Y, Sui S, Chen Q. Mitochondrial outer-membrane protein FUNDC1 mediates hypoxia-induced mitophagy in mammalian cells. Nat Cell Biol. 2012;14:177–185. doi: 10.1038/ncb2422. [PubMed: 22267086]

24. Chen G, Han Z, Feng D, Chen Y, Chen L, Wu H, Huang L, Zhou C, Cai X, Fu C, Duan L, Wang X, Liu L, Liu X, Shen Y, Zhu Y, Chen Q. A regulatory signaling loop comprising the PGAM5 phosphatase and CK2 controls receptor-mediated mitophagy. Mol Cell. 2014;54:362–377. doi: 10.1016/j.molcel.2014.02.034. [PubMed: 24746696]

25. Wu W, Lin C, Wu K, Jiang L, Wang X, Li W, Zhuang H, Zhang X, Chen H, Li S, Yang Y, Lu Y, Wang J, Zhu R, Zhang L, Sui S, Tan N, Zhao B, Zhang J, Li L, Feng D. FUNDC1 regulates mitochondrial dynamics at the ER-mitochondrial contact site under hypoxic conditions. EMBO J. 2016;35:1368–1384. doi: 10.15252/embj.201593102. [PubMed: 27145933]

26. Mathews CE, Langley SH, Leiter EH. New mouse model to study islet transplantation in insulin-dependent diabetes mellitus. Transplantation. 2002;73:1333–1336. doi: 10.1097/00007890-200204270-00024. [PubMed: 11981430]

27. Figueira TR. A word of caution concerning the use of Nnt-mutated C57BL/6 mice substrains as experimental models to study metabolism and mitochondrial pathophysiology. Exp Physiol. 2013;98:1643. doi: 10.1113/expphysiol.2013.074682. [PubMed: 24058187]

28. Ronchi JA, Figueira TR, Ravagnani FG, Oliveira HC, Vercesi AE, Castilho RF. A spontaneous mutation in the nicotinamide nucleotide transhydrogenase gene of C57BL/6J mice results in mitochondrial redox abnormalities. Free Radic Biol Med. 2013;63:446–456. doi: 10.1016/j.freeradbiomed.2013.05.049. [PubMed: 23747984]

29. Gong G, Liu X, Wang W. Regulation of metabolism in individual mitochondria during excitation-contraction coupling. J Mol Cell Cardiol. 2014;76:235–246. doi: 10.1016/j.yjmcc.2014.09.012. [PubMed: 25252178]

30. Dong Y, Zhang M, Liang B, Xie Z, Zhao Z, Asfa S, Choi HC, Zou MH. Reduction of AMP-activated protein kinase alpha2 increases endoplasmic reticulum stress and atherosclerosis in vivo. Circulation. 2010;121:792–803. doi: 10.1161/CIRCULATIONAHA.109.900928. [PubMed: 20124121]

31. Wieckowski MR, Giorgi C, Lebiedzinska M, Duszynski J, Pinton P. Isolation of mitochondria-associated membranes and mitochondria from animal tissues and cells. Nat Protoc. 2009;4:1582–1590. doi: 10.1038/nprot.2009.151. [PubMed: 19816421]

32. Barlow AL, Macleod A, Noppen S, Sanderson J, Guérin CJ. Colocalization analysis in fluorescence micrographs: verification of a more accurate calculation of pearson's correlation

coefficient. Microsc Microanal. 2010;16:710–724. doi: 10.1017/S143192761009389X. [PubMed: 20946701]

33. Bianchi K, Rimessi A, Prandini A, Szabadkai G, Rizzuto R. Calcium and mitochondria: mechanisms and functions of a troubled relationship. Biochim Biophys Acta. 2004;1742:119–131. doi: 10.1016/j.bbamcr.2004.09.015. [PubMed: 15590062]
34. Szabadkai G, Simoni AM, Chami M, Wieckowski MR, Youle RJ, Rizzuto R. Drp-1-dependent division of the mitochondrial network blocks intraorganellar Ca^{2+} waves and protects against Ca^{2+}-mediated apoptosis. Mol Cell. 2004;16:59–68. doi: 10.1016/j.molcel.2004.09.026. [PubMed: 15469822]
35. Bonora M, Morganti C, Morciano G, Giorgi C, Wieckowski MR, Pinton P. Comprehensive analysis of mitochondrial permeability transition pore activity in living cells using fluorescence-imaging-based techniques. Nat Protoc. 2016;11:1067–1080. doi: 10.1038/nprot.2016.064. [PubMed: 27172167]
36. Boutagy NE, Rogers GW, Pyne ES, Ali MM, Hulver MW, Frisard MI. Using isolated mitochondria from minimal quantities of mouse skeletal muscle for high throughput microplate respiratory measurements. J Vis Exp. 2015:e53216. doi: 10.3791/53216. [PubMed: 26555567]
37. Nagai T, Sawano A, Park ES, Miyawaki A. Circularly permuted green fluorescent proteins engineered to sense Ca^{2+}. Proc Natl Acad Sci U S A. 2001;98:3197–3202. doi: 10.1073/pnas.051636098. [PubMed: 11248055]
38. Wendt ER, Ferry H, Greaves DR, Keshav S. Ratiometric analysis of fura red by flow cytometry: a technique for monitoring intracellular calcium flux in primary cell subsets. PloS one. 2015;10:e0119532. doi: 10.1371/journal.pone.0119532. [PubMed: 25835294]
39. Jean-Quartier C, Bondarenko AI, Alam MR, Trenker M, Waldeck-Weiermair M, Malli R, Graier WF. Studying mitochondrial Ca(2+) uptake - a revisit. Mol Cell Endocrinol. 2012;353:114–127. doi: 10.1016/j.mce.2011.10.033. [PubMed: 22100614]
40. Pozzan T, Rudolf R. Measurements of mitochondrial calcium in vivo. Biochim Biophys Acta. 2009;1787:1317–1323. doi: 10.1016/j.bbabio.2008.11.012. [PubMed: 19100709]
41. Santulli G, Xie W, Reiken SR, Marks AR. Mitochondrial calcium increase is a key determinant in heart failure. Proc Natl Acad Sci U S A. 2015;112:11389–11394. doi: 10.1073/pnas.1513047112. [PubMed: 26217001]
42. Lu JP, Wang Y, Sliter DA, Pearce MM, Wojcikiewicz RJ. RNF170 protein, an endoplasmic reticulum membrane ubiquitin ligase, mediates inositol 1,4,5-trisphosphate receptor ubiquitination and degradation. J Biol Chem. 2011;286:24426–24433. doi: 10.1074/jbc.M111.251983. [PubMed: 21610068]
43. Xie Z, Lau K, Eby B, Lozano P, He C, Pennington B, Li H, Rathi S, Dong Y, Tian R, Kem D, Zou MH. Improvement of cardiac functions by chronic metformin treatment is associated with enhanced cardiac autophagy in diabetic OVE26 mice. Diabetes. 2011;60:1770–1778. doi: 10.2337/db10-0351. [PubMed: 21562078]
44. Giorgi C, Missiroli S, Patergnani S, Duszynski J, Wieckowski MR, Pinton P. Mitochondria-associated membranes: composition, molecular mechanisms, and physiopathological implications. Antioxid Redox Signal. 2015;22:995–1019. doi: 10.1089/ars.2014.6223. [PubMed: 25557408]
45. Xie Z, Dong Y, Scholz R, Neumann D, Zou MH. Phosphorylation of LKB1 at serine 428 by protein kinase C-zeta is required for metformin-enhanced activation of the AMP-activated protein kinase in endothelial cells. Circulation. 2008;117:952–962. doi: 10.1161/CIRCULATIONAHA.107.744490. [PubMed: 18250273]
46. Zhou G, Myers R, Li Y, Chen Y, Shen X, Fenyk-Melody J, Wu M, Ventre J, Doebber T, Fujii N, Musi N, Hirshman MF, Goodyear LJ, Moller DE. Role of AMP-activated protein kinase in mechanism of metformin action. J Clin Invest. 2001;108:1167–1174. doi: 10.1172/JCI13505. [PubMed: 11602624]
47. Meng S, Cao J, He Q, Xiong L, Chang E, Radovick S, Wondisford FE, He L. Metformin activates AMP-activated protein kinase by promoting formation of the alphabetagamma heterotrimeric complex. J Biol Chem. 2015;290:3793–3802. doi: 10.1074/jbc.M114.604421. [PubMed: 25538235]

48. Effect of intensive blood-glucose control with metformin on complications in overweight patients with type 2 diabetes (UKPDS 34). UK prospective diabetes study (UKPDS) group. Lancet. 1998;352:854–865. doi: 10.1016/S0140-6736(98)07037-8. [PubMed: 9742977]
49. Ikeda Y, Shirakabe A, Maejima Y, Zhai P, Sciarretta S, Toli J, Nomura M, Mihara K, Egashira K, Ohishi M, Abdellatif M, Sadoshima J. Endogenous Drp1 mediates mitochondrial autophagy and protects the heart against energy stress. Circ Res. 2015;116:264–278. doi: 10.1161/CIRCRESAHA.116.303356. [PubMed: 25332205]
50. Song M, Mihara K, Chen Y, Scorrano L, Dorn GW 2nd. Mitochondrial fission and fusion factors reciprocally orchestrate mitophagic culling in mouse hearts and cultured fibroblasts. Cell Metab. 2015;21:273–285. doi: 10.1016/j.cmet.2014.12.011. [PubMed: 25600785]
51. Puthanveetil P, Wan A, Rodrigues B. FoxO1 is crucial for sustaining cardiomyocyte metabolism and cell survival. Cardiovasc Res. 2013;97:393–403. doi: 10.1093/cvr/cvs426. [PubMed: 23263330]
52. Evans-Anderson HJ, Alfieri CM, Yutzey KE. Regulation of cardiomyocyte proliferation and myocardial growth during development by FOXO transcription factors. Circ Res. 2008;102:686–694. doi: 10.1161/CIRCRESAHA.107.163428. [PubMed: 18218983]
53. Battiprolu PK, Hojayev B, Jiang N, Wang ZV, Luo X, Iglewski M, Shelton JM, Gerard RD, Rothermel BA, Gillette TG, Lavandero S, Hill JA. Metabolic stress-induced activation of FoxO1 triggers diabetic cardiomyopathy in mice. J Clin Invest. 2012;122:1109–1118. doi: 10.1172/jci60329. [PubMed: 22326951]
54. Qi Y, Zhu Q, Zhang K, Thomas C, Wu Y, Kumar R, Baker KM, Xu Z, Chen S, Guo S. Activation of Foxo1 by insulin resistance promotes cardiac dysfunction and beta-myosin heavy chain gene expression. Circ Heart Fail. 2015;8:198–208. doi: 10.1161/circheartfailure.114.001457. [PubMed: 25477432]
55. Hsueh W, Abel ED, Breslow JL, Maeda N, Davis RC, Fisher EA, Dansky H, McClain DA, McIndoe R, Wassef MK, Rabadan-Diehl C and Goldberg IJ. Recipes for creating animal models of diabetic cardiovascular disease. Circulation research. 2007;100:1415–27. doi: 10.1161/01.RES.0000266449.37396.1f. [PubMed: 17525381]
56. Wang J, Takeuchi T, Tanaka S, Kubo SK, Kayo T, Lu D, Takata K, Koizumi A and Izumi T. A mutation in the insulin 2 gene induces diabetes with severe pancreatic beta-cell dysfunction in the Mody mouse. The Journal of clinical investigation. 1999;103:27–37. doi: 10.1172/jci4431. [PubMed: 9884331]
57. Basu R, Oudit GY, Wang X, Zhang L, Ussher JR, Lopaschuk GD, Kassiri Z. Type 1 diabetic cardiomyopathy in the Akita (Ins2WT/C96Y) mouse model is characterized by lipotoxicity and diastolic dysfunction with preserved systolic function. Am J Physiol Heart Circ Physiol. 2009;297:H2096–H2108. doi: 10.1152/ajpheart.00452.2009. [PubMed: 19801494]
58. Fuentes-Antras J, Picatoste B, Gomez-Hernandez A, Egido J, Tunon J, Lorenzo O. Updating experimental models of diabetic cardiomyopathy. J Diabetes Res. 2015;2015:656795. doi: 10.1155/2015/656795. [PubMed: 25973429]
59. Ding WX, Yin XM. Mitophagy: mechanisms, pathophysiological roles, and analysis. Biol Chem. 2012;393:547–564. doi: 10.1515/hsz-2012-0119. [PubMed: 22944659]
60. Xu X, Kobayashi S, Chen K, Timm D, Volden P, Huang Y, Gulick J, Yue Z, Robbins J, Epstein PN, Liang Q. Diminished autophagy limits cardiac injury in mouse models of type 1 diabetes. J Biol Chem. 2013;288:18077–18092. doi: 10.1074/jbc.M113.474650. [PubMed: 23658055]
61. Rizzuto R, De Stefani D, Raffaello A, Mammucari C. Mitochondria as sensors and regulators of calcium signalling. Nat Rev Mol Cell Biol. 2012;13:566–578. doi: 10.1038/nrm3412. [PubMed: 22850819]
62. Denton RM. Regulation of mitochondrial dehydrogenases by calcium ions. Biochim Biophys Acta. 2009;1787:1309–1316. doi: 10.1016/j.bbabio.2009.01.005. [PubMed: 19413950]
63. Cardenas C, Miller RA, Smith I, Bui T, Molgo J, Muller M, Vais H, Cheung KH, Yang J, Parker I, Thompson CB, Birnbaum MJ, Hallows KR, Foskett JK. Essential regulation of cell bioenergetics by constitutive InsP3 receptor Ca^{2+} transfer to mitochondria. Cell. 2010;142:270–283. doi: 10.1016/j.cell.2010.06.007. [PubMed: 20655468]

64. Orrenius S, Zhivotovsky B, Nicotera P. Regulation of cell death: the calcium-apoptosis link. Nat Rev Mol Cell Biol. 2003;4:552–565. doi: 10.1038/nrm1150. [PubMed: 12838338]

65. Joiner ML, Koval OM, Li J, He BJ, Allamargot C, Gao Z, Luczak ED, Hall DD, Fink BD, Chen B, Yang J, Moore SA, Scholz TD, Strack S, Mohler PJ, Sivitz WI, Song LS, Anderson ME. CaMKII determines mitochondrial stress responses in heart. Nature. 2012;491:269–273. doi: 10.1038/nature11444. [PubMed: 23051746]

66. Marchi S, Pinton P. The mitochondrial calcium uniporter complex: molecular components, structure and physiopathological implications. J Physiol. 2014;592:829–839. doi: 10.1113/jphysiol.2013.268235. [PubMed: 24366263]

67. Chalmers S, McCarron JG. The mitochondrial membrane potential and Ca^{2+} oscillations in smooth muscle. J Cell Sci. 2008;121:75–85. doi: 10.1242/jcs.014522. [PubMed: 18073239]

68. Talbot J, Barrett JN, Barrett EF, David G. Stimulation-induced changes in NADH fluorescence and mitochondrial membrane potential in lizard motor nerve terminals. J Physiol. 2007;579:783–798. doi: 10.1113/jphysiol.2006.126383. [PubMed: 17218351]

69. Boyman L, Williams GS, Khananshvili D, Sekler I, Lederer WJ. NCLX: the mitochondrial sodium calcium exchanger. J Mol Cell Cardiol. 2013;59:205–213. doi: 10.1016/j.yjmcc.2013.03.012. [PubMed: 23538132]

70. Palty R, Silverman WF, Hershfinkel M, Caporale T, Sensi SL, Parnis J, Nolte C, Fishman D, Shoshan-Barmatz V, Herrmann S, Khananshvili D, Sekler I. NCLX is an essential component of mitochondrial Na^{+}/Ca^{2+} exchange. Proc Natl Acad Sci U S A. 2010;107:436–441. doi: 10.1073/pnas.0908099107. [PubMed: 20018762]

71. Voccoli V, Tonazzini I, Signore G, Caleo M, Cecchini M. Role of extracellular calcium and mitochondrial oxygen species in psychosine-induced oligodendrocyte cell death. Cell Death Dis. 2014;5:e1529. doi: 10.1038/cddis.2014.483. [PubMed: 25412308]

72. Joseph LC, Barca E, Subramanyam P, Komrowski M, Pajvani U, Colecraft HM, Hirano M, Morrow JP. Inhibition of NAPDH oxidase 2 (NOX2) prevents oxidative stress and mitochondrial abnormalities caused by saturated fat in cardiomyocytes. PloS one. 2016;11:e0145750. doi: 10.1371/journal.pone.0145750. [PubMed: 26756466]

73. Nita II, Hershfinkel M, Fishman D, Ozeri E, Rutter GA, Sensi SL, Khananshvili D, Lewis EC, Sekler I. The mitochondrial Na^{+}/Ca^{2+} exchanger upregulates glucose dependent Ca^{2+} signalling linked to insulin secretion. PloS one. 2012;7:e46649. doi: 10.1371/journal.pone.0046649. [PubMed: 23056385]

74. Minta A, Kao JP, Tsien RY. Fluorescent indicators for cytosolic calcium based on rhodamine and fluorescein chromophores. J Biol Chem. 1989;264:8171–8178. [PubMed: 2498308]

75. Rutter GA, Burnett P, Rizzuto R, Brini M, Murgia M, Pozzan T, Tavare JM, Denton RM. Subcellular imaging of intramitochondrial Ca^{2+} with recombinant targeted aequorin: significance for the regulation of pyruvate dehydrogenase activity. Proc Natl Acad Sci U S A. 1996;93:5489–5494. [PubMed: 8643602]

Clinical Perspective

What is new?

- Diabetes caused aberrant MAM formation and Fundc1 expression in cardiomyocytes.
- Increased formation of Fundc1-associated MAMs resulted in mitochondrial Ca^{2+} increase, mitochondrial fragmentation and mitochondrial dysfunction, and cardiac dysfunction in diabetic hearts.
- Fundc1 promoted diabetic MAM formation by inhibiting Ip_3r2 ubiquitination and proteasome degradation.
- Ampkα2 suppressed Fundc1 and diabetes increased Fundc1 expression by suppressing Ampkα2 activity.

What are the clinical implications?

- The left ventricle cardiac tissues of hearts from patients with clinically diagnosed diabetic cardiomyopathy had higher FUNDC1 than their counterparts from healthy human donor hearts, suggesting a role of FUNDC1 in human diabetic cardiomyopathy.
- Activation of AMPK suppresses FUNDC1 and/or its associated MAM formation in cardiomyocytes.
- Metformin, an AMPK activator used exclusively for type 2 diabetes, might be effective in treating diabetic cardiomyopathy in type 1 diabetes.

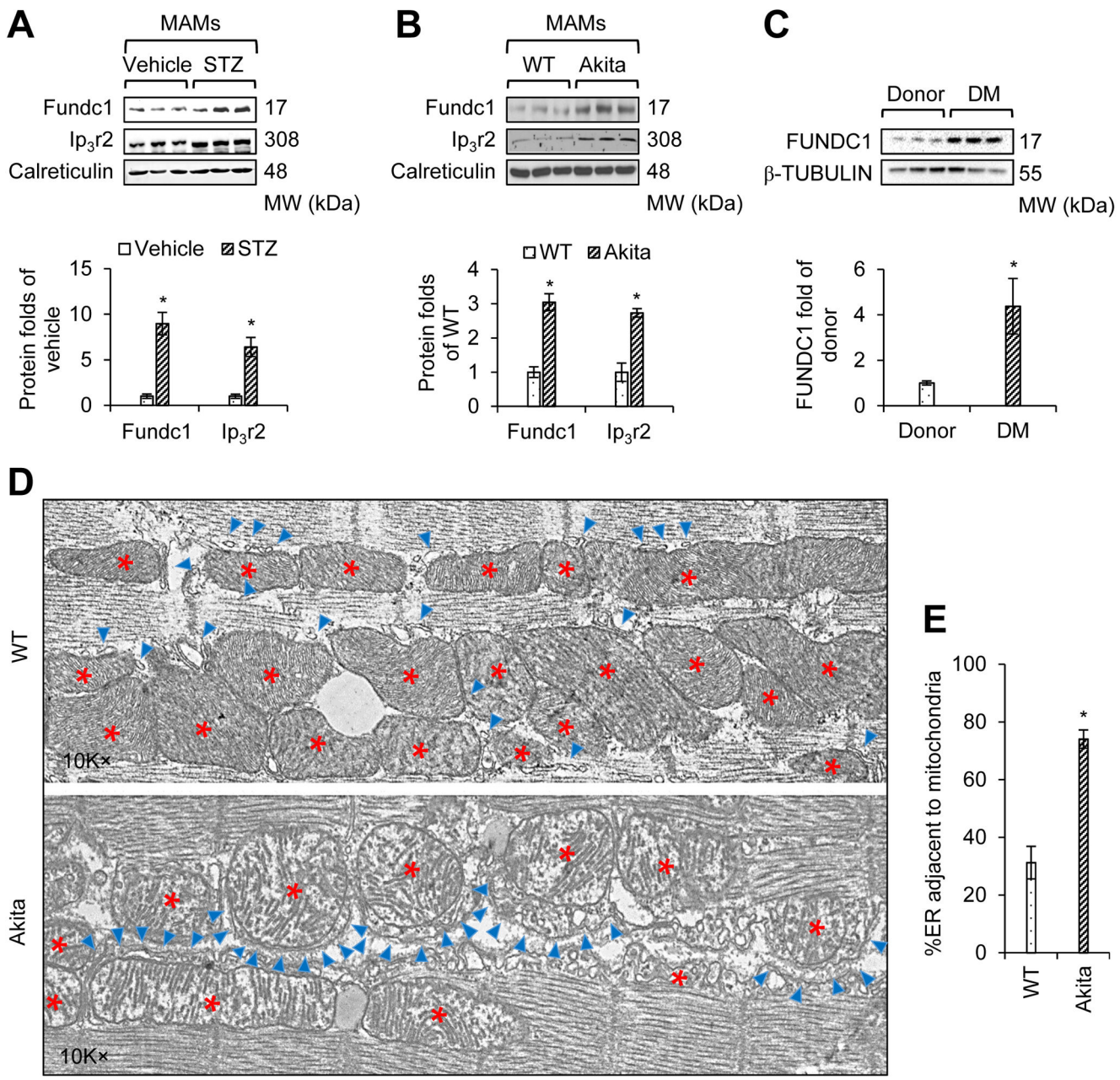

Figure 1. Type 1 diabetes enhances the formation of mitochondria-associated endoplasmic reticulum (ER) membranes (MAMs) in the heart.

A, Western blot analysis of the interest proteins in cardiac MAM fractions prepared from vehicle- or streptozotocin (STZ)-treated mice at the age of 6 months. Lower panel: Densitometric analysis of the blots (mean ± SD, $n = 6\sim7$ mice per group; $^*P < 0.05$ versus vehicle). **B**, Western blot analysis of the interest proteins in cardiac MAM fractions prepared from wild-type (WT) and Akita mice at the age of 6 months. Lower panel: Densitometric analysis of the blots (mean ± SD, $n = 6\sim7$ mice per group; $^*P < 0.05$ versus WT). **C**, Western blot analysis of the interest proteins in cardiac homogenates prepared from donor or diabetes mellitus (DM) patients. Lower panel: Densitometric analysis of the blots (mean ±

SD, $n = 6$ patients per group; $^*P < 0.05$ versus donor). **D**, Representative transmission electron microscope (TEM) images of the ER and mitochondrial morphology in the cardiac muscle of WT and Akita mice at 6 months of age. The red stars indicate mitochondria, and the blue asterisks indicate ER. **E**, A bar graph illustrating the quantitation of ER length adjacent to mitochondria, normalized to total ER length (mean ± SD, $n = 5$~7 mice per group; $^*P < 0.05$ versus WT).

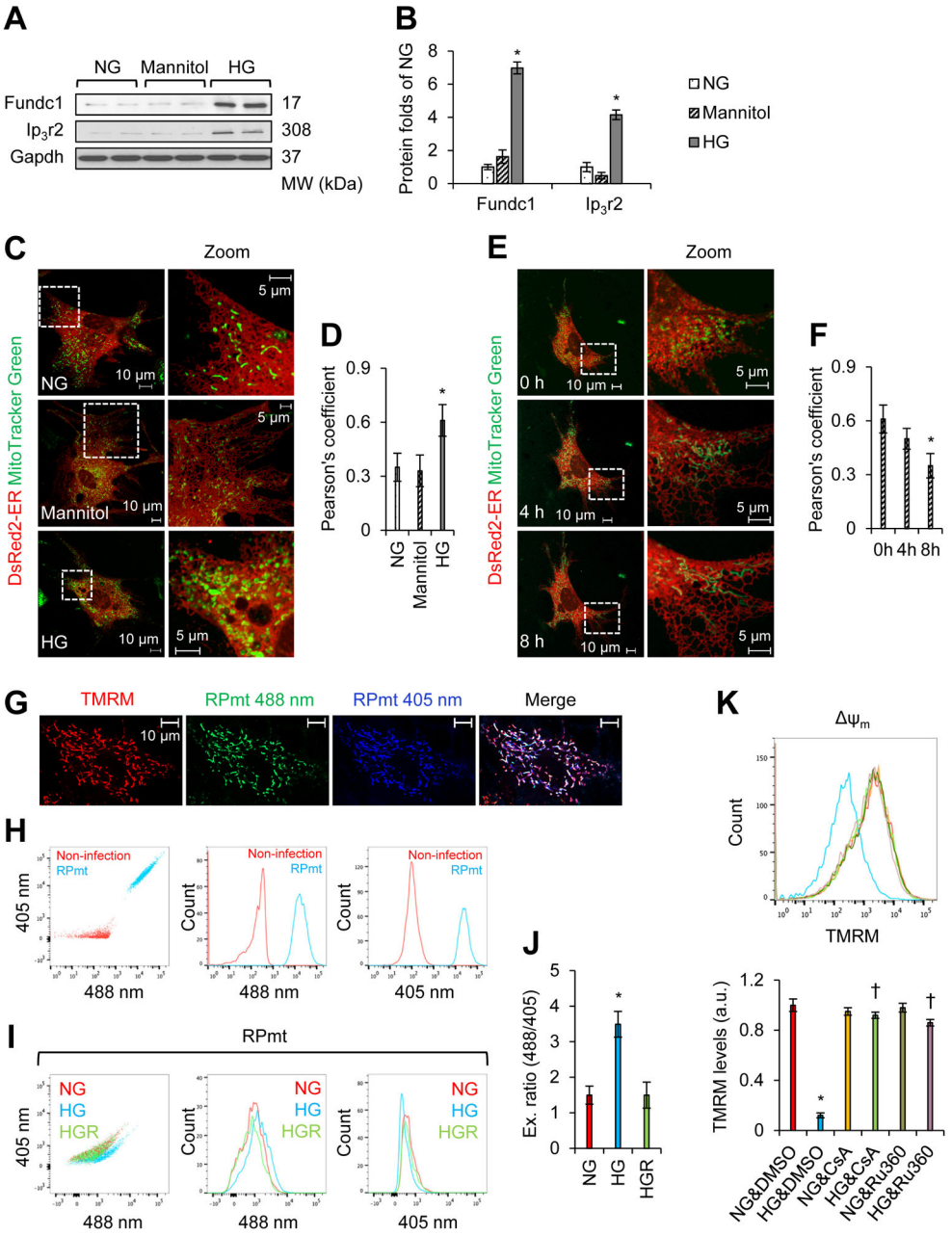

Figure 2. MAMs increase in mouse neonatal cardiomyocytes treated with high glucose (HG).

A, Western blot analysis of the interest proteins in mouse neonatal cardiomyocytes grown in normal glucose (NG, 5.5 mmol/L D-glucose), osmotic control (24.5 mmol/L D-mannitol plus 5.5 mmol/L D-glucose), or HG (30 mmol/L D-glucose) conditions for 48 h. **B**, Densitometric analysis of the blots in **A** (mean ± SD, **P* < 0.05 versus NG). **C**, Association between the ER (DsRed2-ER) and mitochondria (MitoTracker Green) was analyzed by confocal microscopy. Representative images are shown. **D**, Quantitation of ER-mitochondria contacts using the Pearson's coefficient (mean ± SD, **P* < 0.05 versus NG). **E**, Time-lapse confocal microscopy images illustrating associations between the ER and mitochondria. Mouse neonatal cardiomyocytes were cultured in HG (30 mmol/L D-glucose) conditions for

48 h. HG medium was then changed to NG (5.5 mmol/L D-glucose) medium, and the association between ER (DsRed2-ER) and mitochondria (MitoTracker Green) were analyzed. Representative images are shown. **F**, Quantitation of ER-mitochondria contacts using the Pearson's coefficient (mean ± SD, $*P < 0.05$ versus 0 h). **G**, Mitochondrial localization of mitochondrial Ca^{2+} RPmt indicator was demonstrated by tetramethylrhodamine, methyl ester (TMRM) staining. **H**, Flow cytometry (FCM) to determine the infection efficiency of adenovirus PRmt (MOI = 50). Beta-galactosidase (ad-β-Gal, MOI = 50) was used as a control (non-infection). **I and J**, FCM analysis using RPmt infected cells showing mitochondrial Ca^{2+} levels (RPmt) under NG (5.5 mmol/L D-glucose), HG (30 mmol/L D-glucose), and HGR (HG removal for 8 h) conditions. **I**, Representative FCM plots under NG, HG, and HGR conditions. **J**, Excitation ratio of 488/405 in each group (mean ± SD, $*P < 0.05$ versus NG). **K**, Detection of mitochondrial membrane potential ($\Delta\Psi_m$). Cells were first exposed to NG (5.5 mmol/L D-glucose) or HG (30 mmol/L D-glucose) in the presence of DMSO (control reagent), cyclosporine A (CsA, 1 μmol/L), or Ru360 (10 μmol/L). $\Delta\Psi_m$ was assayed by using the TMRM probe. Upper panel: Representative FCM plots. Lower panel: TMRM levels in each group (mean ± SD, $*P < 0.05$ versus NG & DMSO; $^{\dagger} P < 0.05$ versus HG & DMSO).

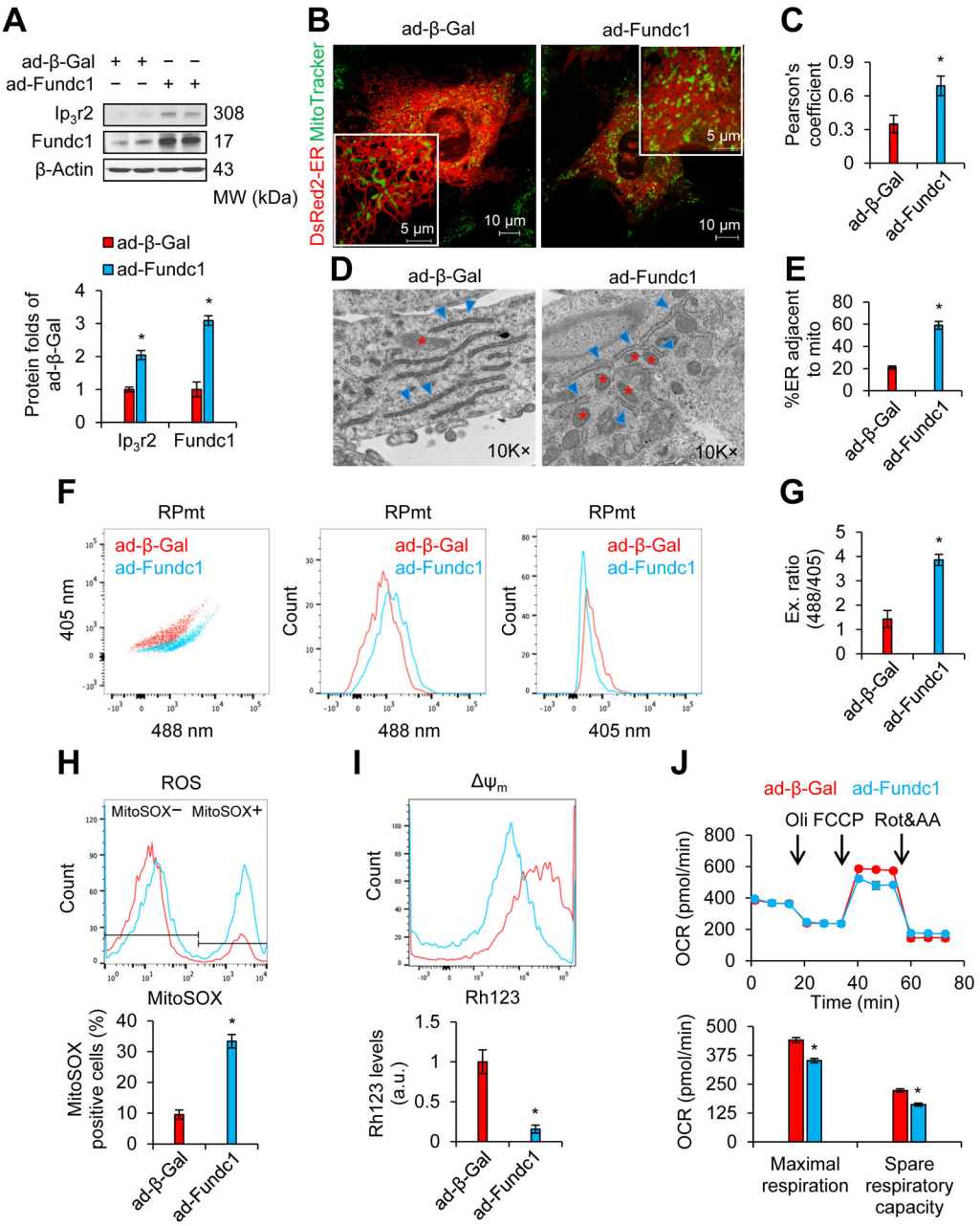

Figure 3. Adenovirus-mediated overexpression of *FUN14 domain containing 1* (*Fundc1*) increases MAM formation and induces mitochondrial dysfunction in mouse neonatal cardiomyocytes.

Mouse neonatal cardiomyocytes (**A-C**; **F-J**) or H9c2 rat myoblasts (**D and E**) were infected with adenoviruses encoding Fundc1 (ad-Fundc1) or beta-galactosidase (ad-β-Gal) for 48 h. **A**, Proteins of interest were assayed by western blot. Densitometric analysis of the blots is shown in the lower panel (mean ± SD, **P* < 0.05 versus ad-β-Gal). **B**, Confocal images illustrating the association between the ER (DsRed2-ER) and mitochondria (MitoTracker Green). Representative images are shown. **C**, Quantitation of ER-mitochondria contacts using the Pearson's coefficient (mean ± SD, **P* < 0.05 versus ad-β-Gal). **D**, Representative

TEM images of ER and mitochondrial morphology are shown. The red stars indicate mitochondria, and the blue asterisks indicate ER. **E**, Quantitation of ER length adjacent to mitochondria, normalized to total ER length (mean ± SD, $*P < 0.05$ versus ad-β-Gal). **F**, FCM analysis illustrating mitochondrial Ca^{2+} levels using the RPmt indicator. Representative FCM plots are shown. **G**, The excitation ratio of 488/405 in each group (mean ± SD, $*P < 0.05$ versus ad-β-Gal). **H**, Representative FCM plots quantifying levels of reactive oxygen species (ROS) using the MitoSOX probe (upper panel) and histograms of the percentage of MitoSOX-positive cells in the indicated groups (lower panel) (mean ± SD, $*P < 0.05$ versus ad-β-Gal). **I**, Representative FCM plots illustrating mitochondrial membrane potential ($\Delta\Psi_m$) using the rhodamine 123 (Rh123) probe (upper panel). Intensities of Rh123-stained cells are quantified in the lower panel (mean ± SD, $*P < 0.05$ versus ad-β-Gal). **J**, Upper panel: Graph illustrating oxygen consumption rate (OCR), measured using a Seahorse extracellular flux analyzer. Lower panel: Quantitation of maximal respiration and spare respiratory capacity (mean ± SD, $*P < 0.05$ versus ad-β-Gal).

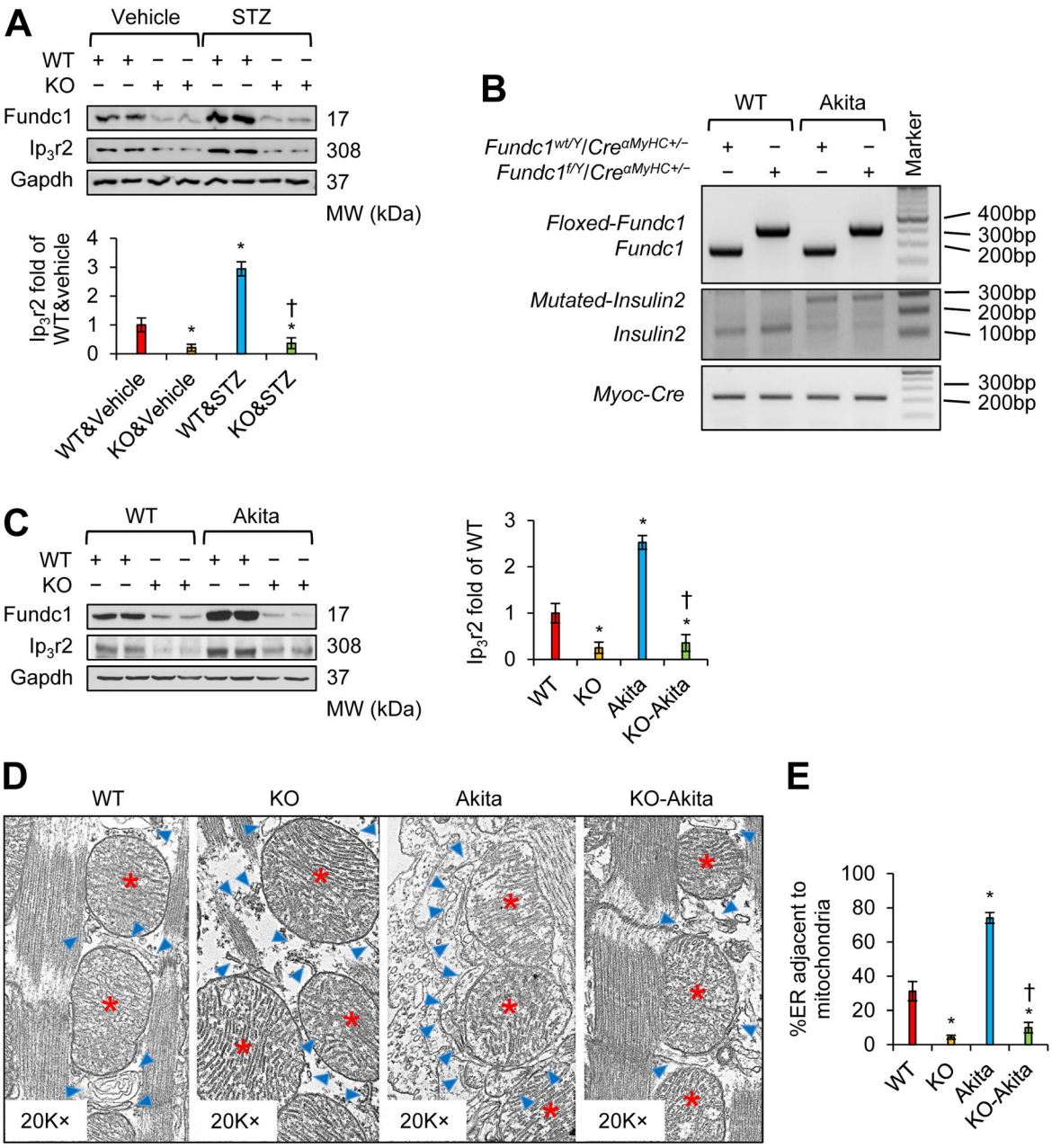

Figure 4. Cardiac-specific *Fundc1* knockout (KO) inhibits diabetes-induced MAM formation.

A, Western blot analysis of the interest proteins in cardiac homogenates prepared from vehicle- or STZ-treated WT or cardiac *Fundc1* KO mice at the age of 6 months. Densitometric analysis of the blots is shown in the lower panel (mean ± SD, $n = 8$ mice per group; $^{*}P < 0.05$ versus WT & vehicle; $^{\dagger}P < 0.05$ versus WT & STZ). **B**, Genotyping results illustrating cardiac-specific *Fundc1* deletion in Akita mice. **C**, Western blot analysis of the interest proteins in cardiac homogenates from WT, *Fundc1* KO, Akita, and *Fundc1* KO Akita mice at the age of 6 months. Densitometric analysis of the blots is shown in the right panel (mean ± SD, $n = 8$ mice per group; $^{*}P < 0.05$ versus WT; $^{\dagger}P < 0.05$ versus Akita). **D**, Representative TEM images of ER and mitochondrial morphology in the cardiac muscle of

WT, *Fundc1* KO, Akita, and *Fundc1* KO Akita mice at the age of 6 months. The red stars indicate mitochondria, and the blue asterisks indicate ER. **E**, Quantitation of ER length adjacent to mitochondria, normalized to total ER length (mean ± SD, $n = 5\sim7$ mice per group; $^{*}P < 0.05$ versus WT; $^{\dagger}P < 0.05$ versus Akita).

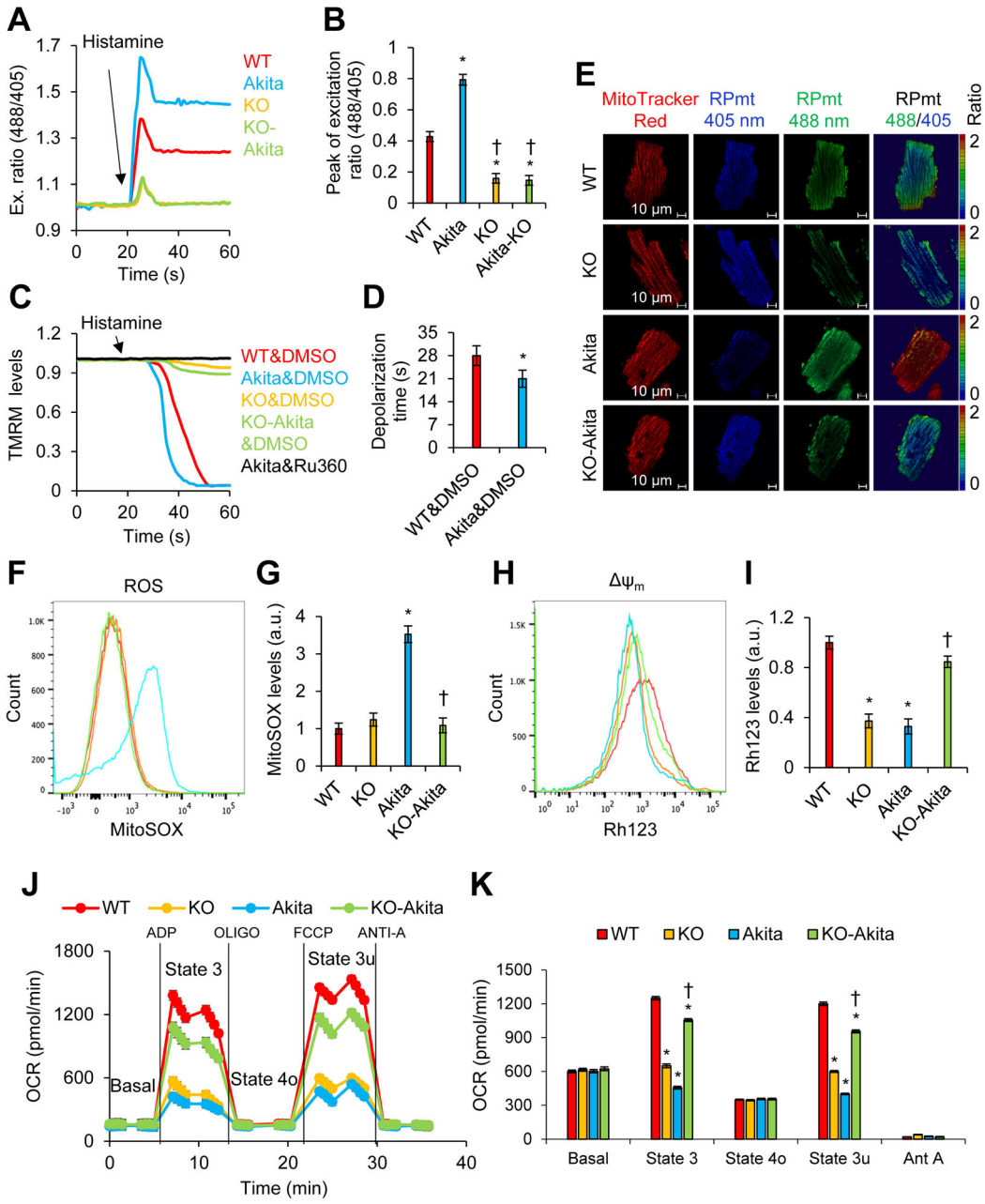

Figure 5. Cardiac-specific *Fundc1* KO prevents mitochondrial Ca^{2+} increase and improves mitochondrial function in Akita hearts.

A, Representative curves of the time course of mitochondrial Ca^{2+} uptake after histamine (100 μmol/L) stimulation in adult cardiomyocytes from WT, *Fundc1* KO, Akita, and *Fundc1* KO Akita mice. The mitochondrial Ca^{2+} levels were indicated by ratiometric pericam (RPmt). The basal lines were normalized to 1. **B**, Summary data show the peak levels of mitochondrial Ca^{2+} uptake in A (mean ± SD, n = 6~7 mice per group, 10 cells from each heart were used; *P < 0.05 versus WT; †P < 0.05 versus Akita). **C**, The representative time course for histamine (100 μmol/L)–induced mitochondrial membrane potential ($\Delta\Psi_m$). Adult cardiomyocytes from WT, *Fundc1* KO, Akita, and *Fundc1* KO Akita mice were

incubated with DMSO (control reagent) or Ru360 (10 μmol/L). The $\Delta\Psi_m$ levels were indicated by TMRM probe. The basal lines were normalized to 1. **D**, Summary data show the time of mitochondrial depolarization in WT cells and Akita cells (mean ± SD, $n = 8$ mice per group, 20 cells from each heart were used for statistical analysis; $^*P < 0.05$ versus WT & DMSO). **E**, Confocal images illustrating the resting mitochondrial Ca^{2+} levels using RPmt indicator in mouse adult cardiomyocytes. Representative images are shown. **F-I**, Representative FCM plots of (**F**) mitochondrial ROS levels (MitoSOX), and (**H**) mitochondrial membrane potential (Rh123) in cardiac mitochondria isolated from 8-week-old WT, *Fundc1* KO, Akita, and *Fundc1* KO Akita mice. Histograms of the (**G**) intensities of MitoSOX-stained cells (mean ± SD, $n = 5$~7 mice per group; $^*P < 0.05$ versus WT; $^\dagger P < 0.05$ versus Akita), and (**I**) intensities of Rh123-stained cells (mean ± SD, $n = 5$~7 mice per group; $^*P < 0.05$ versus WT; $^\dagger P < 0.05$ versus Akita). **J**, Graph illustrating mitochondrial coupling assay measured using a Seahorse extracellular flux analyzer. **K**, Quantitation of OCR in different states (mean ± SD, $n = 8$ mice per group; $^*P < 0.05$ versus WT; $^\dagger P < 0.05$ versus Akita).

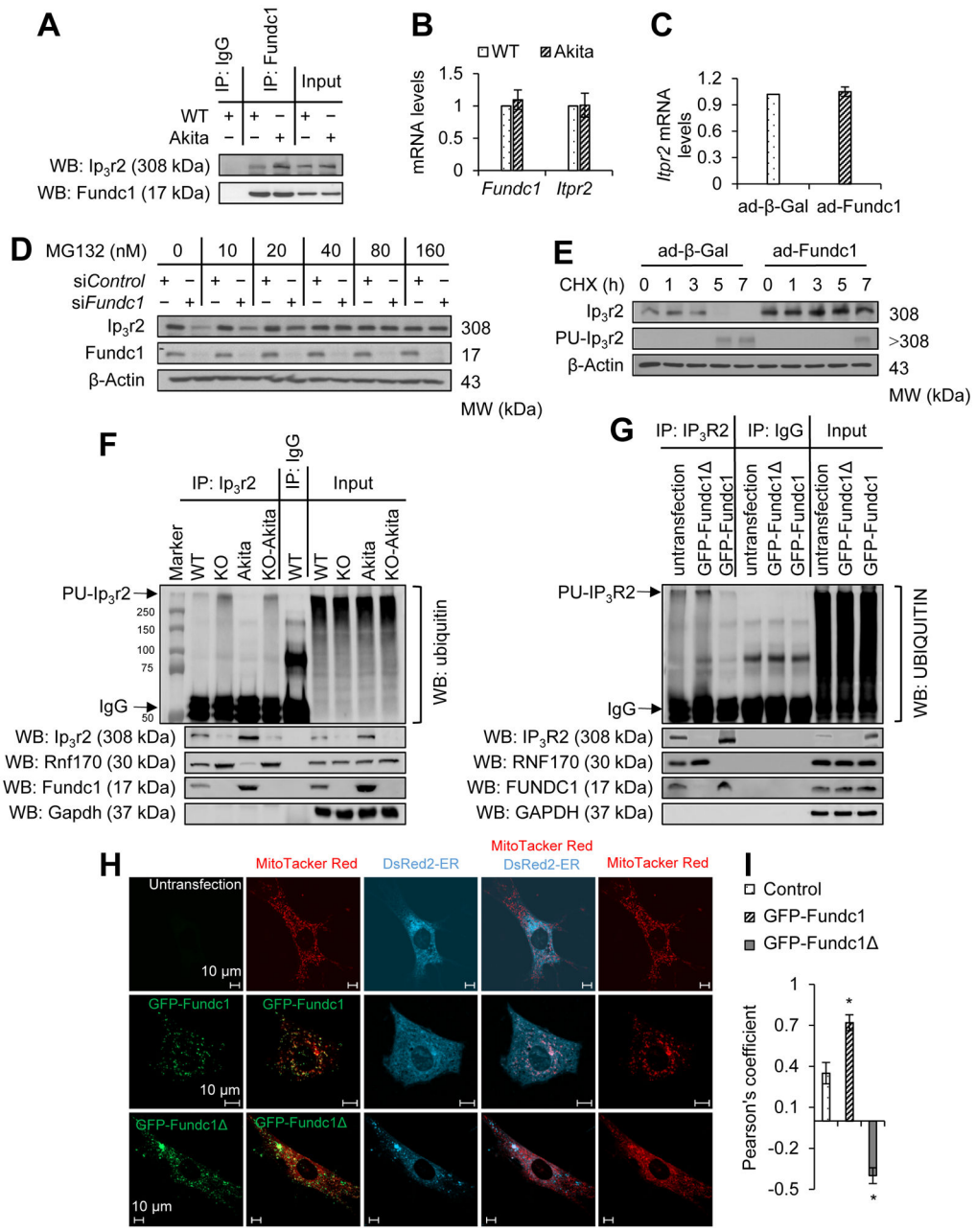

Figure 6. Fundc1 inhibits Ip$_3$r2 ubiquitination and degradation.

A, The interaction between Ip$_3$r2 and Fundc1 in WT and Akita hearts (6-month-old) was detected by immunoprecipitation (IP) and western blot (WB). **B**, Message RNA (mRNA) levels of *Itpr2* (the gene encoding Ip$_3$r2) and *Fundc1* in WT and Akita hearts were measured by quantitative reverse transcription polymerase chain reaction (RT-PCR) (mean ± SD, $n = 8$ mice per group). **C**, RT-PCR quantitation of *Itpr2* mRNA levels in mouse neonatal cardiomyocytes infected with ad-β-Gal or ad-Fundc1 for 48 h (mean ± SD). **D**, Western blot analysis for Ip$_3$r2 and Fundc1 in mouse neonatal cardiomyocytes transfected with *control* siRNA (si*Control*) or *Fundc1* siRNA (si*Fundc1*) for 48 h and treated with MG132 at the indicated dose. **E**, Western blot analysis of Ip$_3$r2 in mouse neonatal cardiomyocytes infected

with ad-β-Gal or ad-Fundc1 for 48 h, and treated with 200 μmol/L of cycloheximide (CHX) for the indicated time. Polyubiquitination of Ip_3r2 (PU-Ip_3r2) was determined by IP of Ip_3r2 and subsequent blotting for ubiquitin. **F**, Results of IP experiments from cardiac homogenates in WT, *Fundc1* KO, Akita, and *Fundc1* KO Akita mice. Anti-Ip_3r2 IP was followed by western blotting for ubiquitin to determine levels of PU-Ip_3r2. The protein levels of ring finger protein 170 (Rnf170), Ip_3r2, and Fundc1 in the precipitates were determined with protein-specific primary antibodies ($n = 8$ mice per group). **G**, 293T cells were transfected with GFP-Fundc1 or a Fundc1 truncation plasmid (GFP-Fundc1Δ7-48) for 24 h, and the cell lysate was subjected to IP for Ip_3r2. PU-Ip_3r2 was determined following western blotting for ubiquitin and proteins of interest in the precipitates were detected using protein-specific primary antibodies. **H**, Representative confocal images illustrating the contacts between ER (DsRed2-ER) and mitochondria (MitoTracker Red) in mouse neonatal cardiomyocytes transfected with the GFP-Fundc1 or GFP-Fundc1Δ7-48 plasmid for 48 h. **I**, Quantitation of ER-mitochondria contacts using the Pearson's coefficient (mean ± SD, $*P < 0.05$ versus control).

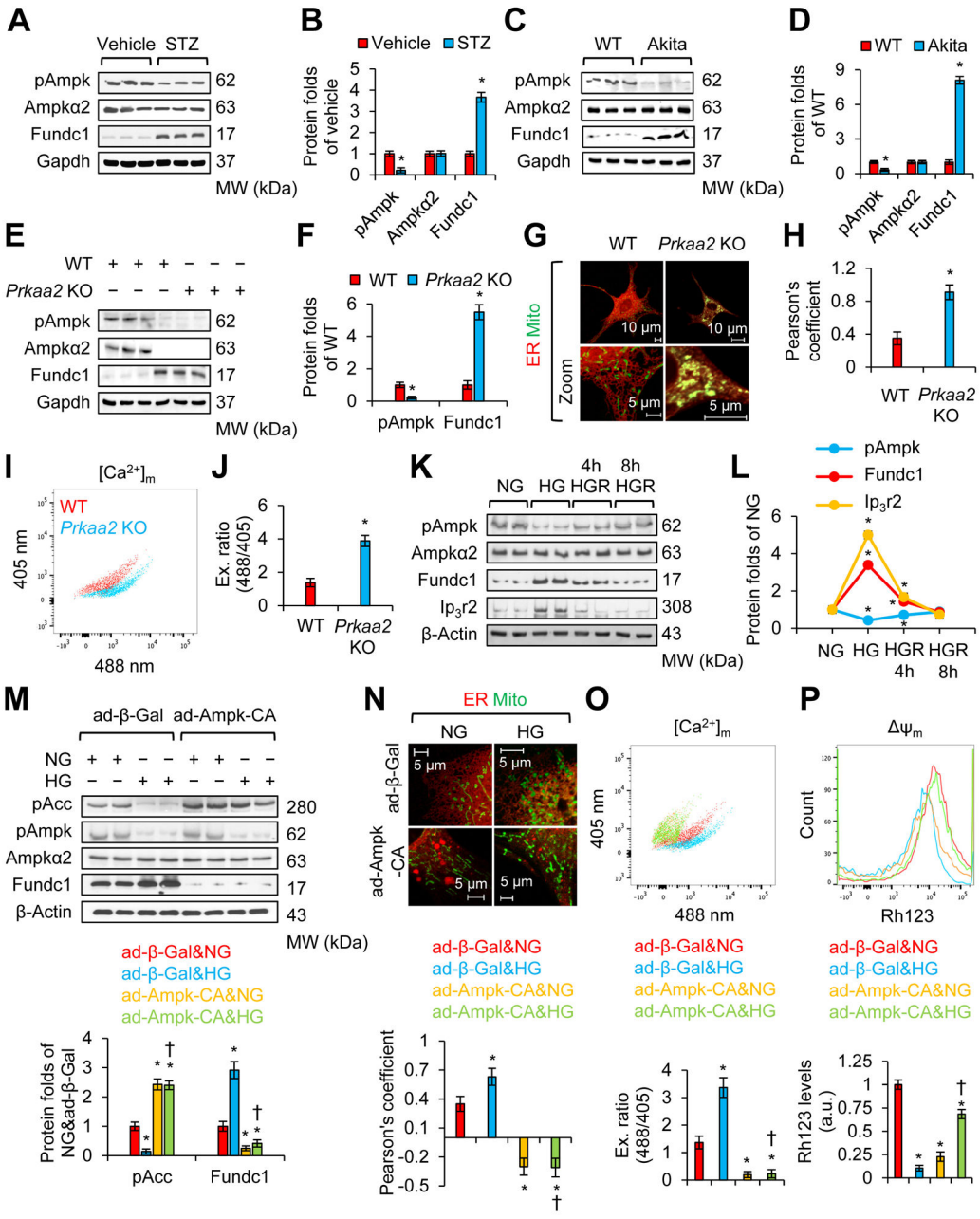

Figure 7. Diabetes increases Fundc1 by downregulating AMP-activated protein kinase (Ampk).

A, Western blot analysis for the interest proteins in cardiac homogenates prepared from the vehicle or STZ-treated mice at 6 months. **B**, Densitometric analysis of blots in **A** (mean ± SD, $n = 8$ mice per group; $^*P < 0.05$ versus vehicle). **C**, Western blot analysis for the interest proteins of interest in cardiac homogenates prepared from WT and Akita mice at 6 months. **D**, Densitometric analysis of blots in **C** (mean ± SD, $n = 8$ mice per group; $^*P < 0.05$ versus WT). **E**, Western blot analysis for proteins of interest in cardiac homogenates prepared from WT and *Prkaa2* (gene encoding Ampkα2) KO mice at 6 months. **F**, Densitometric analysis of blots in **E** (mean ± SD, $n = 8$ mice per group; $^*P < 0.05$ versus WT). **G**, Representative confocal images illustrating the association between the ER (DsRed2-ER) and mitochondria

(MitoTracker Green) in WT or *Prkaa2* KO mouse neonatal cardiomyocytes. **H**, Quantitation of ER and mitochondrial contacts using Pearson's coefficient (mean ± SD, $n = 5$ mice per group; $^{*}P < 0.05$ versus WT). **I**, Representative FCM plots illustrating mitochondrial Ca^{2+} levels using the RPmt indicator. **J**, Excitation ratio of 488/405 in each group (mean ± SD, $n = 8$ mice per group; $^{*}P < 0.05$ versus WT). **K**, Western blot analysis for the interest proteins in mouse neonatal cardiomyocytes grown in NG (5.5 mmol/L D-glucose), osmotic control (24.5 mmol/L D-mannitol plus 5.5 mmol/L D-glucose), or HG (30 mmol/L D-glucose) conditions for 48 h. HGR group: Forty-eight hours after HG treatment, cells were cultured in NG for the indicated time. **L**, Densitometric analysis of blots in **K** (mean ± SD, $^{*}P < 0.05$ versus NG). **M-P**, Mouse neonatal cardiomyocytes were infected with ad-β-Gal or constitutively active mutant Ampk (ad-Ampk-CA), and received NG (5.5 mmol/L D-glucose) or HG (30 mmol/L D-glucose) treatment. **M**, Proteins of interest were assayed by western blot. Lower panel: Densitometric analysis of blots (mean ± SD, $^{*}P < 0.05$ versus ad-β-Gal & NG; $^{\dagger}P < 0.05$ versus ad-β-Gal & HG). **N**, The association between the ER (DsRed2-ER) and mitochondria (MitoTracker Green) was analyzed by confocal microscopy. Upper panel: Representative images are shown. Lower panel: ER and mitochondrial contacts are quantitated using the Pearson's coefficient (mean ± SD, $^{*}P < 0.05$ versus ad-β-Gal & NG; $^{\dagger}P < 0.05$ versus ad-β-Gal & HG). **O**, Mitochondrial Ca^{2+} levels were determined by FCM using RPmt indicator. Upper panel: Representative FCM plots. Lower panel: Histogram of the excitation ratio of 488/405 in each group (mean ± SD, $^{*}P < 0.05$ versus ad-β-Gal & NG; $^{\dagger}P < 0.05$ versus ad-β-Gal & HG). **P**, Mitochondrial membrane potential ($\Delta\Psi_m$) was determined by FCM using the Rh123 probe. Upper panel: Representative FCM plots. Lower panel: The intensities of Rh123-stained cells (mean ± SD, $^{*}P < 0.05$ versus ad-β-Gal & NG; $^{\dagger}P < 0.05$ versus ad-β-Gal & HG).

Table 1.

Echocardiography values in WT and *Fundc1* KO mice with STZ or control vehicle treatment.

	WT&Vehicle	KO&Vehicle	WT&STZ	KO&STZ
EF (%)	66.82±4.27	58.93±3.14 *	59.83±3.85 *	65.67±2.81 †
FS (%)	37.43±3.43	30.98±2.67 *	32.12±2.73 *	35.76±1.72 †
E/A	1.95±0.22	1.51±0.25 *	1.42±0.21 *	1.87±0.23 †
IVRT (ms)	16.05±0.51	21.04±0.72 *	21.38±0.77 *	15.38±0.74 †
IVS;d (mm)	0.68±0.11	0.67±0.07	0.68±0.13	0.70±0.14
IVS;s (mm)	0.84±0.12	0.87±0.24	0.82±0.14	0.86±0.21
LVID;d (mm)	4.16±0.21	4.53±0.27 *	4.48±0.26 *	4.23±0.24 †
LVID;s (mm)	3.14±0.19	3.29±0.29 *	3.30±0.38 *	3.21±0.19 †
LVPW;d (mm)	0.63±0.17	0.67±0.21	0.71±0.21	0.79±0.23
LVPW;s (mm)	0.80±0.21	0.82±0.23	0.87±0.24	0.90±0.23
HR (bpm)	438.73±42.63	429.55±17.99	455.61±22.78	443.39±41.05

The value represents mean ± SD, n = 5~8 mice per group

* $P < 0.05$ versus WT & vehicle

† $P < 0.05$ versus WT & STZ. Ejection fraction (EF); Fractional shortening (FS); Isovolumic relaxation time (IVRT); E-wave and A-wave represent the LV early filling and atrial contraction filling, respectively (E/A-wave ratio); Interventricular septal end diastole (IVS; d) and end systole (IVS; s); Left ventricular internal diameter end diastole (LVID; d) and end systole (LVID; s); Left ventricular posterior wall end diastole (LVPW; d) and end systole (LVPW; s); Heart rate (HR).

Table 2.

Echocardiography values in WT, *Fundc1* KO, Akita, and *Fundc1* KO Akita mice.

	WT	KO	Akita	KO-Akita
EF (%)	67.33±5.15	56.64±4.17 *	60.14±8.12	64.48±7.87
FS (%)	37.48±6.26	30.31±3.87 *	32.79±5.11	34.44±4.47
E/A	1.83±0.28	1.27±0.22 *	1.51±0.37	1.67±0.31
IVRT (ms)	15.18±3.21	20.98±4.15 *	20.31±4.32 *	15.79±3.07 †
IVS;d (mm)	0.64±0.11	0.71±0.12	0.68±0.09	0.72±0.12
IVS;s (mm)	0.81±0.17	0.84±0.16	0.91±0.15	0.91±0.14
LVID;d (mm)	4.11±0.31	4.31±0.39 *	4.26±0.48	4.29±0.48
LVID;s (mm)	3.09±0.28	3.36±0.39 *	3.08±0.60	3.16±0.42
LVPW;d (mm)	0.62±0.17	0.69±0.19	0.67±0.19	0.71±0.22
LVPW;s (mm)	0.78±0.19	0.80±0.21	0.83±0.19	0.89±0.21
HR (bpm)	433.82±37.24	438.54±31.24	441.32±36.75	448.74±35.66

The value represents mean ± SD, n = 6~8 mice per group

* $P < 0.05$ versus WT

† $P < 0.05$ versus Akita.